Field Performance of Scour Protection Around Offshore Monopiles

T.C. Raaijmakers[1], M.C. van Oeveren[2], D. Rudolph[3], V. Leenders[4], W.C.P. Sinjou[5]

[1]Deltares | Delft Hydraulics, Rotterdamseweg 185, P.O. Box 177, 2600 MH Delft, The Netherlands; e-mail:tim.raaijmakers@deltares.nl
[2]Deltares | Delft Hydraulics, Rotterdamseweg 185, P.O. Box 177, 2600 MH Delft, The Netherlands; e-mail:claire.vanoeveren@deltares.nl
[3]Deltares | Delft Hydraulics, Rotterdamseweg 185, P.O. Box 177, 2600 MH Delft, The Netherlands; e-mail:daniel.rudolph@deltares.nl
[4]Ballast Nedam Beheer B.V., Amersfoortsestraat 124d, P.O. Box 50, 3769 ZH Soesterberg, The Netherlands; e-mail: v.leenders@ballast-nedam.nl
[5]Ballast Nedam Beheer B.V., Amersfoortsestraat 124d, P.O. Box 50, 3769 ZH Soesterberg, The Netherlands; e-mail: w.sinjou@ballast-nedam.nl

ABSTRACT

Offshore Windpark Egmond aan Zee was installed in 2006 and is the first Dutch offshore windpark. To guarantee a fixed seabed level, dynamic scour protections were installed at all 36 monopiles. Since installation 251 multibeam surveys were executed to investigate the as-built stages and yearly performance of the dynamic scour protection. After 4 major storms the onset of deformation was observed around the monopiles: rocks within 1 pile diameter from the pile centre are displaced to a ring within 1-1.5 pile diameter from the pile centre. The majority of the deformation, however, was attributed to overall compaction of the armour layer. Performance parameters based on two design formulae were calculated for the actual occurred hydrodynamics and compared with the observed deformation. Both predictions performed well, although there are differences in the sensitivity to the hydrodynamic parameters. Consequently, the ranking of the severity of the storms was different for both approaches.

INTRODUCTION

The European offshore wind energy market is booming. In 2009 a growth rate of 54% was achieved. For 2010, a market growth of 75% is expected (*press release EWEA, 2010*). To establish such growth numbers, the wind energy market will have to focus more and more on cost efficiency, design optimization, flexible building methods and more reliable risk assessments. One relatively small, though important link in the chain of offshore wind park construction concerns the bed protection around the foundations to prevent scour development. Now, after a few years of operation of one of the first offshore windparks (the Dutch Offshore Windpark Egmond aan Zee, hereafter OWEZ), we have the opportunity to investigate the performance of the bed protection, which was designed on the basis of laboratory tests, in the field.

OWEZ is located approximately 10 to 18 kilometres from Egmond aan Zee, off the Dutch coast, at water depths varying between 16 and 21 metres relative to MSL. It consists of 36 wind turbine generators (hereafter WTG) with a total capacity of 108 MW and an anticipated lifetime of 20 years. The foundations of the turbines consist of monopiles with an outer diameter of 4.6 meter.
In order to maintain the designed fixation level, scour protection was applied. The scour protection system comprises two layers: a granular filter layer and a dynamically stable armour layer, see Figure 1.

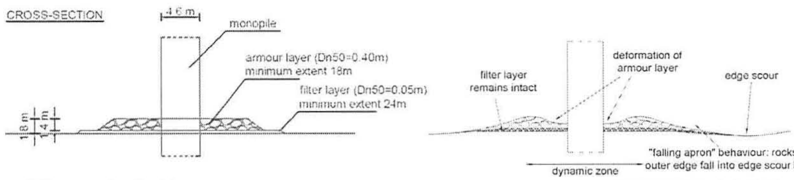

Figure 1: (left) scour protection layout for all 36 WTGs of OWEZ; (right) expected deformation pattern

Experiments were conducted to verify several conceptual protection layouts. In this laboratory test program it was found that the deformation of the scour protection followed a characteristic pattern as shown in the right plot of Figure 1. Some armour material is moved from close to the pile to a few meters away but does not disappear out of the vicinity of the pile. Just outside the scour protection edge scour develops. The scour protection behaves as a falling apron and partially rolls in the edge scour hole. The deepest edge scour hole develops at the downstream side of the main current direction. For the layout shown in Figure 1, a lowering of the top level of the armour of about 0.4m (range 0.3m to 0.6m, depending on the location in the windpark) was predicted in case the 100 year design storm occurred. For the finally chosen design, an edge scour depth of 1-2m was expected, based on the interpretation of laboratory experiments and engineering judgement.

This paper focuses on design and performance of so-called dynamic scour protections around monopiles. The analysis is based on bathymetric surveys and hydrodynamic data at OWEZ (both measurements and operational models). In section 2 an overview of literature on scour protection for offshore wind parks is presented. Section 3 describes the as-built situation and performance of the scour protections on the basis of 251 bathymetric surveys, executed in the period 2006-2009. In section 4 the observations are correlated to the hydrodynamic climate. Also some prediction formulae for deformation of the scour protection are evaluated. Finally, in section 5 the conclusions and recommendations are presented. Although edge scour development is important in relation to burial depth of electricity cables and deformation of the edges of the scour protection, this topic is not further addressed in this paper.

LITERATURE ON SCOUR PROTECTIONS

Some years ago some excellent books on scour (Whitehouse (1998), Sumer and Fredsoe (2002), Hoffmans and Verheij (1997)), were published. More recently, formulations for scour around monopiles in the marine environment were further improved (Raaijmakers, 2008) and time-dependent scour development around monopiles in field conditions can be predicted with reasonable accuracy (Rudolph, 2008). However, most of the times, the predicted scour depths are considered to be unacceptable. A scour protection is then required to guarantee a certain fixation level. Besides more innovative (and consequently not fully proven) techniques, like artificial frond mats, collars and gabions, the most reliable and scientifically proven method to protect the seabed is a protection consisting of loose rock. In general, the following types of rock protection are distinguished:

I. **Static protection**, in which the rocks in the armour layer are statically stable (i.e. do not move) during the design condition.

II. **Dynamic protection**, in which some stone movement is allowed as long as the structure will not fail. Three different types of dynamic protections can be identified:

- IIa. **Fully dynamic protection**, in which the (usually small) rocks fully interact with the mobile seabed. During severe wave-dominated conditions rocks are picked up within the wave cycles and seabed sediment is washed out before the rocks fall back onto the seabed. Consequently, still a scour hole will develop, but the scour depth and timescale are smaller resp. larger than without the presence of bed protection.
- IIb. **Later installed dynamic protection**, which is installed after a scour hole developed around the structure. The protection material is assumed to be sufficiently stable to prevent further scouring of the seabed.
- IIc. **Slightly dynamic protection**, which is installed on the initial seabed and allows for evolving towards a dynamic profile as long as the deformation remains limited to the top layer.

A Type-I protection is installed at Horns Rev windfarm (Den Boon, 2004). Type-IIa protections are not very popular for wind turbines, since the fixation depth will vary in time, which results in varying resonance frequencies. In the offshore oil&gas industry. Type-IIa protections are often applied for temporary drilling operations, where strict requirements are applied for the maximum stone size and scour development is acceptable as long as the penetration depth is not exceeded (Raaijmakers, 2007).

Type-IIb protections guarantee a constant fixation level after some time, when the scour protection is installed. The pile length of course has to accommodate for some scouring. However, because the top level of the protection is almost flush with the surrounding seabed, the loads on the protection are generally lower. Examples are Scroby Sands and Princess Amalia Windpark. At OWEZ, a Type-IIc protection is installed, which guarantees a fixed initial seabed level, the shortest possible pile length and the lowest possible burial depth for electricity cables. Since the scour protection protrudes approximately 2 to 3m above the seabed, the hydrodynamic loads are somewhat larger. All types of rock protection usually are designed on the basis of the bed shear stress approach. A well-documented overview of design formulae is presented in De Vos (2008). Most formulae are available for current-only situations (e.g. bridge piers in rivers), but some formulae exist for wave-dominated conditions.

For offshore (wave-dominated) conditions, Den Boon (2004) and Whitehouse (2006) describe the OPTI-PILE design tool, which calculates a stability parameter:

$$\mathrm{Stab} = \frac{\theta_{\max}}{\theta_{\mathrm{cr}}}$$

in which θ_{max} = maximum Shields parameter and θ_{cr} = critical Shields parameter. From model tests it was found that for values of Stab < 0.415 no movement of the stones in the scour protection occurred; for 0.415 ≤ Stab < 0.460 some movement occurred but no failure and for Stab ≥ 0.460 the scour protection failed. Note that this failure criterion is not dependent on the applied rock volume, although applying a larger volume can still be a viable alternative: a larger deformation will occur during severe conditions, but this will not be problematic as long as the deformation is restricted to the scour protection.

De Vos (2008) presents a formula for a damage parameter S_{3D}, which was fitted to 80 test results:

$$\frac{S_{3D}}{N_w^{b_0}} = a_0 \frac{U_m^3 T_{m-1,0}^2}{\sqrt{gh_w}\,(s-1)^{3/2} D_{n50}^2} + a_1 \left[a_2 + a_3 \frac{\left(U_c / w_s \right)^2 (U_c + a_4 U_m)^2 \sqrt{h_w}}{g D_{n50}^{3/2}} \right]$$

in which N_w = number of waves, U_m = wave orbital velocity at the seabed, $T_{m-1,0}$ = spectral wave period (m_0/m_1), g = gravitational constant, h_w = water depth, s = specific density (ρ_s/ρ_w), D_{n50} = nominal stone diameter, U_c = depth-averaged current velocity, w_s = particle fall velocity, b_0 = 0.24300, a_0 = 0.00076, a_2 = -0.02200, a_3 = 0.00790, a_4 = 1 for waves directed with the current and a_4 = Ur/6.4 for waves opposing the current (Ur = Ursell number). Coefficient a_1 = 0 for $U_c/\sqrt{(gD_{n50})}$ < 0.92 *and* for waves directed with the current and a_1 = 1 for $U_c/\sqrt{(gD_{n50})} \geq 0.92$ *or* for waves opposite to the current.

This formula predicts deformation as function of number of waves. Because of the formula shape, deformation will never reach an equilibrium. However, many scour-related formulations predict development towards an equilibrium, as long as the layer characteristics remain constant (i.e. if the armour layer is not fully eroded). To be able to use this formula with the in-house developed software tool OSCAR (Offshore SCour And Remedial measures) for scour predictions, the left part of the formula of De Vos (2008) was slightly modified into:

$$\frac{S_{3D}}{N_w^{b_0}} \approx \frac{S_{3D}}{b_1\left[1-\exp\left(-\frac{N_w}{N_{char}}\right)\right]}$$

which yields similar results within the range N_w = 1000-5000 waves for which the original formula was fitted, when b_1 = 7.6 and the characteristic number of waves N_{char} = 855 waves. This latter value implies that deformation hardly increases after 2500-3000 waves and that equilibrium can be reached within one storm (compare N_{char} = 630 in Raaijmakers, 2007). Only a more severe storm will then be able to reshape the deformation pattern. Note that the De Vos-formula takes the current and wave magnitude and direction into account as well as the stone stability. The formula was fitted for an extent of 5 times the pile diameter D and a layer thickness of $2.5D_{n50}$. The rock volume, height of the protection and pile diameter are not taken into account.

SURVEY ANALYSIS

Multibeam echo sounding surveys were carried out before and after dumping of filter and armour material in 2006. Since 2007 annual surveys have been executed to check the performance of the scour protection. In 2007 at 20 of the 36 WTGs some additional scour protection was installed. In Table 1 an overview of all 251 available surveys is presented. From these surveys, the installed volumes of filter and armour (both initial in 2006 and additional in 2007) material were calculated.

Table 1: Overview of 251 available surveys (as-built and performance checks)

survey ID	survey description	avrg survey date	# surveyed WTGs
SU01	initial seabed	May 2006	33 / 36
SU02	out survey filter 2006	June 2006	36 / 36
SU03	control survey 2006	June 2006	3 / 36
SU04	in survey armour 2006	July 2006	15 / 36
SU05	out survey armour 2006	October 2006	36 / 36
SU06	check survey 2007	June 2007	36 / 36
SU07	out survey additional installed armour	August 2007	20 / 36
SU08	check survey 2008	May 2008	36 / 36
SU09	check survey 2009	May 2009	36 / 36

The average levels within an area with a diameter of 4D are graphically presented in Figure 2. At the negative y-axis the average drop of the scour protection height between 2006 and 2009 is presented for each WTG. Despite some scatter, a weak correlation was found between installed volume (and thus larger obstruction height) and the level drop. The average armour layer thickness still ranges between 1.3 and 1.9m, which is about 3.6 to 5.3 stone layers.

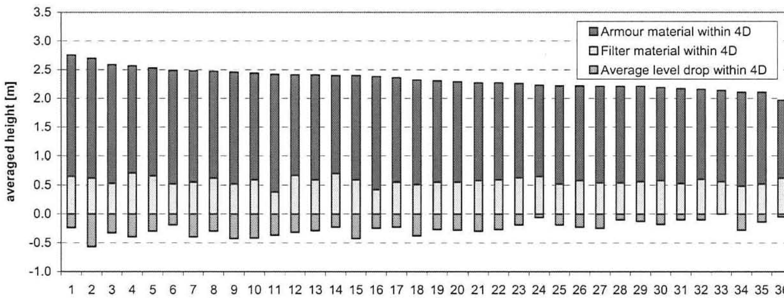

Figure 2: Installed volumes of filter and armour material and averaged bed level drop; WTGs sorted by total installed protection

Direct comparison between model tests and field data is often difficult, because in model tests scour protection layouts are 'perfectly' applied (constant extent and height), whereas the installation in the field is somewhat less accurate.

Often only a minimum layer thickness and extent are defined, which results in local surpluses of scour protection material, both in height and extent. Consequently, the deformation pattern around an individual WTG is very much dependent on the shape and volume of installed protection and it is difficult to draw conclusions on individual piles. Moreover, the correction for the vertical reference level in bathymetric surveys is often based on tidal elevations; an error in the order of 0.10m is easily made. Since the OWEZ-scour protection is designed for a return period of 100 year, it is very likely that the observed deformations during less severe storms are of the same order as possible errors. Therefore, we translated all 36 surveys to one coordinate system (relative to the pile centre) and calculated z-levels relative to the initial seabed. Now we are able to average the results over WTGs that experienced a "similar history". In this way, local variations due to installation inaccuracies and errors in the vertical reference levels are levelled out. In Table 2 the subdivided pile groups are presented.

Table 2: Groups of WTGs with a similar history and therefore comparable

groupID	description of group of WTG's	#WTG's
1	SU05 *before* 2006-storm and *no* additional armour in 2007	3
2	SU05 *after* 2006-storm and *no* additional armour in 2007	12
3	SU05 *before* 2006-storm and additional armour in 2007	9
4	SU05 *after* 2006-storm and additional armour in 2007	8
5	Armour surplus in SW-quadrant	1
6	Filter initially installed NE of intended pile location	1
7	Pile was installed before filter layer	1
8	Only northern part of armour layer was initially installed	1

The total installed scour protection, the present state and the level changes between 2006 and 2009 are plotted for group 2 in Figure 3. It can be observed that the filter layer is indeed nicely installed within an area with diameter 6D and the armour layer within 4D. The middle graph shows a slightly deformed shape of the protection: a somewhat higher armour ring between a diameter of 2-4D, with the highest peak at a diameter of 3D.

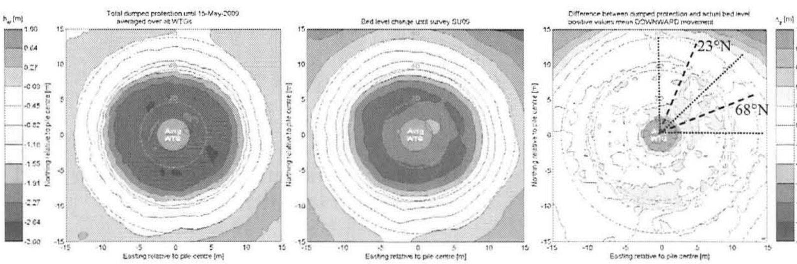

Figure 3: (left) total installed scour protection in 2006; (middle) present state of scour protection and surrounding seabed in 2009; (right) difference between total installed protection and present state; results are averaged over all 12 WTGs in WTG-group 2.

The right plot shows that in the area where the armour was located an average level drop occurred of about 0.25m. Close to the pile (within an area of 2D) this level drop was on average about 0.35m. These observations are also illustrated in Figure 4, which shows cross-sections averaged over 45°-"pie parts". The bold black line shows the 360°-average. Furthermore, all profiles show a local steep part at a distance of about 10m from the pile centre, where some armour rocks at the edge of the armour protection were relocated towards the toe of the armour protection. Further away from the side slope of the armour layer, the height of the filter layer nearly remained constant, except for 'ray 23°'. This is caused by edge scour development at the north-western side of the pile, which at OWEZ is downstream of the pile with respect to the flood current. The filter material acts as a falling apron as illustrated in Figure 1.

Because the bed level change is so evenly distributed over the armour layer, while the armour layer boundaries still remain rather confined, it seems more likely that the majority of the level changes is not caused by storm-induced reshaping of the protection. In the model tests, this evenly distributed level drop was not observed. Possible causes are compaction of the armour layer, settlement of the soil underneath due to the increased load and mixing of filter an armour material at the interface between the two layers, or a combination. The armour layer in the model tests was compactly installed, whereas installation with a backhoe in the field possibly resulted in a lower initial density and subsequent compaction during the first months. There was no evidence for loss of seabed sediment through the pores of the filter layer, since there was no deformation at locations where only filter material was present (see the area at a distance of 11-15m from the pile centre, excluding 'ray 23°'). Based on the above it was assessed that only about 0.10m (on average, with locally larger deformation) of the average 0.35m can be contributed to storm-induced deformation. The expected inverse correlation between deformation and water depth was too weak to be significant.

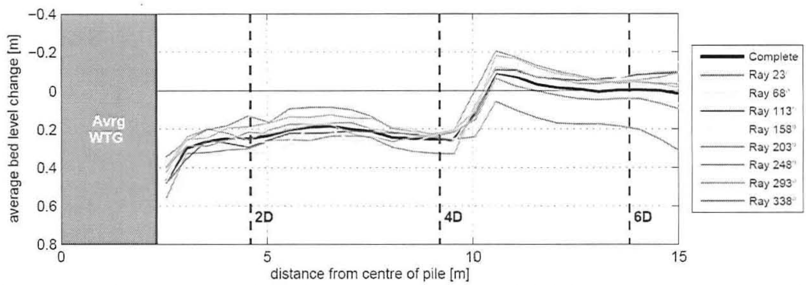

Figure 4: Cross-sectional profiles, averaged over 45°-"pie parts" and averaged over all 12 WTG's in group 2.

HYDRODYNAMIC CLIMATE AND PERFORMANCE PREDICTION

For the evaluation of the performance of the scour protection, a coherent data set consisting of time series of significant wave height (H_s), peak wave period (T_p), mean wave direction (MWD), water level elevation including tide and surge (h_{tot}), depth-averaged current velocity (U_c) and current direction (U_{dir}) was constructed from both measurements and operational models. Since the wave conditions are most important for deformation to the scour protection, only time series of the significant wave height are presented for illustrative purposes in Figure 5.

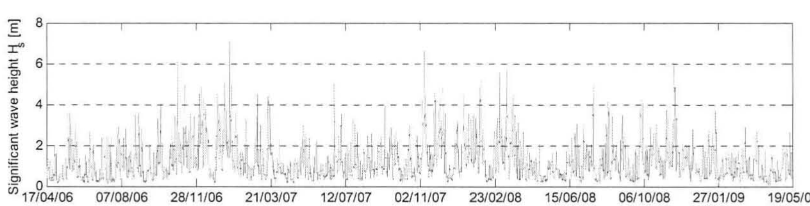

Figure 5: Time series of significant wave height during operational period (until survey SU09) at OWEZ

The most severe storms are presented in Table 3, which also shows the estimated return period for the significant wave height. Note that the time interval of the time series is only 10min, whereas the return periods are calculated on 3hr-storm durations and for nearby measuring station "IJmuiden Munitiestortplaats" (YM6).

Table 3: Storm occurrences between 2006 and 2009, based on $H_{s;peak}$>6.0m, which roughly corresponds to a return period of about 2.0yr at nearby measuring station YM6. Presented values are peak values and as such not representative for the storm duration.

date	10min - H_s [m]	3hr-H_s at YM6 [m]	Return Period (H_s) [yr]	10min - T_p [s]	Stab [-] (OPTI-PILE)	$S_{eq; deVos}$ [m]	$S_{cum}(t)_{; deVos}$ [m]
01-11-2006	6.11	6.87	11.1	16.7	0.30-0.36	0.45-0.76	0.22-0.38
18-01-2007	7.12	5.97	2.0	11.1	0.33-0.42	0.13-0.24	0.22-0.38
09-11-2007	6.64	6.43	4.6	16.7	0.31-0.37	0.30-0.51	0.23-0.40
21-11-2008	6.07	6.56	5.8	11.1	0.30-0.37	0.11-0.27	0.23-0.40

All relevant hydrodynamic parameters were then used to calculate values for the Stab-parameter (see Figure 6) and the predicted deformation according to the formulae by De Vos (see Figure 7). The calculated parameters in Table 3 are presented for a water depth range of 16-20m, in which the highest values correspond to the smallest water depths. When the Stab-parameters are compared with the critical Stab-values, it appears that the OPTI-PILE approach only predicts some deformation of the protection during the storm of 18 January 2007 and only at the shallowest WTG's.

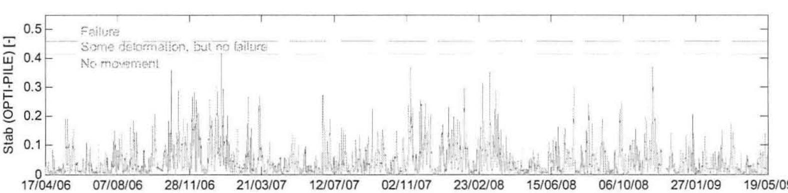

Figure 6: Time series of Stab-values at OWEZ for a water depth of 16m (shallowest WTG-locations)

The conclusion from Figure 7 is somewhat different: the most severe storms occurred at 1 November 2006 and 9 November 2007, although both storms, even with an infinite persistence would not have caused failure of the bed protection. The difference between both formulations is caused by the sensitivity to wave height and wave period. The OPTI-PILE approach takes both parameters into account via the Stab-parameter, in which the wave height is most influential. The presence of the monopile is only accounted for by means of fitting of the critical Stab-values. The hydrodynamic load on the stones around a monopile, however, is also strongly influenced by the type and strength of vortices that are caused by the interaction between hydrodynamics and structure.

The dimensionless Keulegan-Carpenter number ($KC=U_mT/D$) is a good measure to account for interaction between structure and (wave-induced) hydrodynamics. For KC<1 hardly any vortices occur; for 1<KC<6 the lee wake vortices are dominant, while for KC>6 horseshoe vortex development starts. For a given pile diameter D, the hydrodynamic load by vortices is, thus, strongly related to the wave period. This effect is not incorporated in the OPTI-PILE approach.

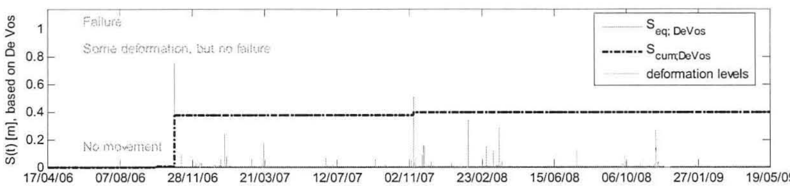

Figure 7: Time series of predicted deformation, according to the slightly modified formula of De Vos.

The approach of De Vos attributes much more weight to the wave period (a power of 2 on the wave period and also through the bed orbital velocity). Although the physical basis for the shape of this formula is not so obvious, this formula implicitly takes the KC-effect into account (through the wave period). The pile diameter is not a variable in the formula, probably because the pile diameter was not varied in the test program to which the formula was fitted. The formula is therefore expected to perform less well for different D/h_w-ratios (and hence a different KC-range).

When the blue lines in Figure 6 and Figure 7 are compared, the sensitivity to the wave period is probably underestimated in the OPTI-PILE approach, while it seems to be somewhat overestimated in the approach of De Vos. It appears that the KC-numbers during the storms of 1 November 2006 and 9 November 2007 were outside the tested range of De Vos. It is therefore not unlikely that the strong dependency on the wave period that was found for the KC-range between 1 to 3 weakens for larger KC-numbers.

Based on the analysis of the performance of both formulae, currently a new formula is being developed that includes the stone stability (through the Stab-parameter), the structure-induced vortex pattern (through the KC-number), the time effect (number of waves), the obstruction height of the protection (ratio h_{obs}/h_w) and the effect of a superimposed current (through the relative velocity and the direction between current and waves).

CONCLUSIONS

In summer/autumn 2006, the 36 monopile foundations of the Egmond windpark were protected with a dynamic scour protection. Since installation in 2006, 4 major storms have occurred with a return period of more than 2 years. The observed deformation from bathymetric surveys was assessed to be mainly related to (a combination of) compaction of the armour layer due to cyclic loading, settlement of the underlying soil and mixing of filter and armour material at the interface between filter and armour layer (average 0.25m). Storm-induced deformation, resulting in a somewhat higher ring of armour stones at a distance of 1-2D from the pile centre, could be observed in the surveys. The storm-related part of the level drop close to the pile ranged between 0 and 0.4m (average 0.10m).

Two formulations (OPTI-PILE and De Vos) were verified against the observations and the deformations all were in the range of the formula predictions, considering the relatively large spread. However, the sensitivity to the wave period was rather different for the two approaches, especially for large KC-numbers. Consequently, the ranking of the severity of the storms was different for both formulae.

For scientific reasons, a storm with a return period closer to the design value would be of interest to extend the verification to "near-failure" situations. Finally, it is concluded that the scour protection behaviour is according to expectations from the model tests at a scale of 1:40, which confirms that model testing is a suitable method for verification of conceptual layouts and design optimisation for dynamic scour protections.

ACKNOWLEDGEMENTS

The authors are thankful to the Dutch Ministry of Economic Affairs for co-financing this research project. Furthermore we would like to thank the contractor Bouwcombinatie Egmond (joint venture of Ballast Nedam and Vestas) and the owner Noordzeewind (a 50/50 joint Venture of Shell and NUON) for providing all bathymetric surveys.

REFERENCES

Boon, J.H. den, Sutherland J., Whitehouse R., Soulsby, R., Stam, C.J., Verhoeven, K., Hogedal, M., Hald, T. (2004). "Scour behaviour and scour protection for monopile foundations of offshore wind turbines". *Proc. European Wind Energy Conferenc*e. London 2004.

Hoffmans, G.J.C.M., Verheij, H.C. (1997). "Scour Manual". *Balkema*, Rotterdam, The Netherlands.

Raaijmakers, T.C., Rudolph, D. (2007). "Scour protection of spud cans - a new design approach". *Proc. of Eleventh Intl. Conference "The Jack-up Platform", Design Construction and Operation*. London, 2007.

Raaijmakers, T.C., D. Rudolph, (2008). Time-dependent scour development under combined current and waves conditions - laboratory experiments with online monitoring technique. *Proc. 4th Intl. Conference on Scour and Erosion*, Tokyo, Japan

Rudolph, D., Raaijmakers, T.C., Stam, C.J.M., (2008), "Time-dependent scour development under combined current and wave conditions – hindcast of field measurements". *Proc. 4th Intl. Conference on Scour and Erosion*, Tokyo, Japan, 2008

Sumer, B.M., Freds¢e, J (2002). "The mechanics of scour in the marine environment". *Advanced Series on Ocean Engineering - Volume 17*. New Jersey: World Scientific.

Vos, L. de, (2008). "Optimisation of scour protection design for monopiles and quantification of wave run-up - Engineering the influence of an offshore wind turbine on local flow conditions". *PhD Thesis* Ghent University.

Whitehouse, R.J.S. (1998), Scour at marine structures. London: Thomas Telford Ltd.

Whitehouse, R.J.S., Sutherland, J., O'Brien, D. (2006). "Seabed scour assessment for offshore windfarm". *Proc. of Third Intl. Conference on Scour and Erosion,* Amsterdam, The Netherlands.

Scour Protection Around Offshore Wind Turbines. Monopiles

A. W. Nielsen[1], B. M. Sumer[2], J. FredsØe[3] and E. D. Christensen[4]

[1] Technical University of Denmark, DTU Mekanik, Section of Coastal, Maritime and Structural Engineering, Building 403, 2800 Kgs. Lyngby, Denmark; e-mail: awni@mek.dtu.dk

[2] Technical University of Denmark, DTU Mekanik, Section of Coastal, Maritime and Structural Engineering, Building 403, 2800 Kgs. Lyngby, Denmark; e-mail: bms@mek.dtu.dk

[3] Technical University of Denmark, DTU Mekanik, Section of Coastal, Maritime and Structural Engineering, Building 403, 2800 Kgs. Lyngby, Denmark; e-mail: jf@mek.dtu.dk

[4] DHI, Agern Allé 5, 2970 Hørsholm, Denmark; e-mail: edc@dhigroup.com

ABSTRACT

The flow processes in a scour protection around a mono-pile in steady current is described in relation to transport of sediment in the scour protection based on physical model tests. Transport of sediment in the scour protection may cause sinking of the scour protection. This may reduce the stability of the mono-pile and change for instance the natural frequency of the dynamic response of an offshore wind turbine in an unfavorable manner. The most important flow process with regard to transport of sediment and sinking of the scour protection is found to be the horseshoe vortex.

It is found that a larger pile diameter relative to the size of the protection stones will cause a larger sinking and that two layers of stones will decrease the sinking relative to one layer of stones with the same size.

INTRODUCTION

During the last decade more and more wind farms have been erected offshore. One of the first larger offshore wind farms is the Horns Rev I. The Horns Rev I is located in relatively shallow water (6.5 to 13 m water (MSL)) about 20 km off the Danish West Coast in the North Sea. This area is exposed to strong tidal currents and large waves from the North Sea. The wind turbines are founded on mono-piles with a scour protection made of a two-layer cover (quarry run from around 350 mm to 550 mm) and a 0.5 m thick filter layer (sea stones from around 30 mm to 200 mm) between the armor layer and the seabed. The wind farm was installed in the summer 2002. A control survey in 2005 showed that the scour protections adjacent to the mono-piles sank up to 1.5 m. This was unexpected and shortly after the survey in 2005 the holes were repaired by adding additional stones.

Scour around unprotected piles have been studied extensively over the last decades. Most of the available results are compiled in Breusers and Raudkivi (1991), Hoffmans and Verheij (1997), Melville and Coleman (2000) (mostly river application), Whitehouse (1998) and Sumer and Fredsøe (2002) (mostly marine application). Scour protection of piles has not been studied nearly as much and the mechanism of failure of scour protections around a mono-pile has only been described briefly. In order to gain an understanding of the mechanisms that cause the sinking of the scour protection, an extensive program of physical model tests with steady current has been carried out in the present study, in an attempt to contribute to the knowledge obtained recently by Chiew and Lim (2000), Lauchlan and Melville (2001), Chiew (2002), De Vos (2008) among others. The model tests showed that the horseshoe vortex, the key element to cause scour around unprotected piles, see e.g. Dargahi (1989) and Roulund et al. (2005), is a key flow feature governing the sinking process.

EXPERIMENTAL SETUP

The tests were conducted in two different current flumes. (1) A 2 m wide, 23 m long (excluding in- and outlet sections) and 0.5 m deep flume; and (2) a 4 m wide, 28 m long (excluding in- and outlet sections) and 1.0 m deep flume. The flumes were equipped with recirculation pumps providing mean current speeds of more than 60 cm/s in the actual setups. Two different setups were used for the tests in the 2 m wide flume: A fixed bottom setup used for flow visualizations and velocity profiles measurements, and a live-bed test setup with a 10 m long and 0.15 m deep sand section, see Figure 1. The ramps towards the sand section were made of smooth plywood plates. In the case of the 4 m wide flume only live-bed tests were conducted. The sand section was around 10 m long and 0.35 m deep. The ramp from the actual bottom to the sand section was 3 m long with a core of concrete blocks covered with at least one layer of stones (d_{50}=4 cm), see Figure 2. In some of the tests in the 4 m wide flume, two piles were tested at the same time, in order to save time. The piles were placed at the same distance from the inlet and the distance between the piles was 1.75 m, which was large enough to ensure no interference.

In the case of the fixed-bottom experiments an approximately 0.5 cm thick, 2.9 m long, white plastic plate, with 15 cm long tapered upstream edge, was placed on the base bottom over the entire width of the flume enabling a good contrast for the flow visualizations. For the velocity profile measurements (using Laser Doppler Anemometry, LDA) the plate was painted matte black to reduce reflections of the laser beams. The pile was placed 2.0 m downstream of the upstream edge of the plastic plate (approximately 15 m from the inlet section).

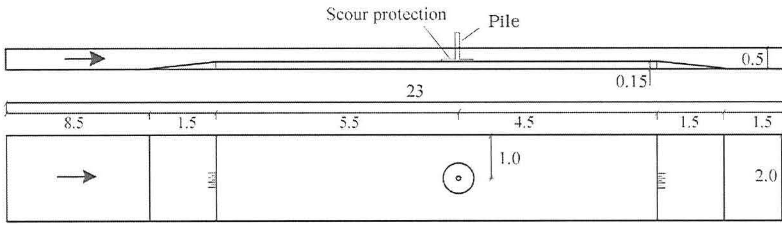

Figure 1 Setup for the 2 m wide flume.

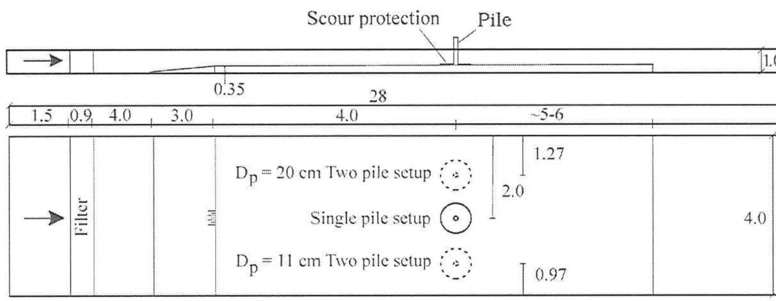

Figure 2 Setups for the 4 m wide flume.

In all setups the bottom end of the piles were closed by an end plate to ensure that the bottom of the pile was completely sealed.

The flow velocity was measured in two different ways: A small propeller (3 cm in diameter) was used in the case of the live-bed tests and a submerged pen size LDA probe was used in the case of the fixed-bottom velocity profiles measurements. The pen-size LDA probe was a two component probe, approximately 1 cm in diameter and 15 cm long. It had a focal length of 80 mm (in water), a beam spacing of 8 mm and a beam diameter of 0.27 mm. The probe was placed vertically pointing downwards, when used to measure velocities in between the stones and placed horizontally when used outside the stones.

The sinking of the stones was determined by measuring the vertical displacement of the stones adjacent to the pile. To avoid disturbances due to the irregularities of the stones the sinking was measured with reference to the same point marked on the stone. In case of large rotations or if the stone was covered by other stones the measuring of the sinking of that stone was disregarded. In the case when a disregarded stone was likely to be the stone with maximum sinking the entire test was disregarded. Based on the results of the tests it was found that the maximum sinking always occurred for the stone upstream of the pile or on the sides of the pile (stone positions 1, 2, 3, 7 and 8 in Figure 3). The number of stones where the sinking was measured around the pile was between three and eight for each test. In the case of only three stones were measured, these were 1, 3 and 7.

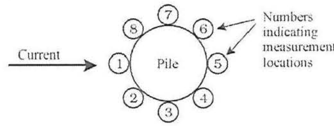

Figure 3 Position of the stones used for measuring the sinking of the scour protection.

Along with the sinking of the stone adjacent to the pile, the scouring and deposition of sand in the area around the pile was measured using measuring pins (3 mm in diameter) with scales in the form of colored strips. The pins were placed in and around the scour protection.

TEST CONDITIONS

One sand size was used for the experiments, d_{50}=0.18 mm. The pile diameter, D_p, was changed in the interval 7.5 cm to 20.0 cm. The extent of the scour protection, w_{cover}, was kept in the interval of 20 to 90 cm giving a relative extension of the scour protection, w_{cover}/D_p, of 2.0 to 4.5, in which w_{cover} is the plan-view extension of the scour protection from upstream edge to downstream edge. The size of the cover stones, D_{cover}, was in the interval 1.9 cm to 10.3 cm (d_{50}) and applied in one to three layers. The water depth, h, was maintained at 29 cm to 30 cm and at 56 cm, giving a relative water depth, h/D_p, of 2.1 to 5.1. The velocity, $U_{D/2}$, at half the pile diameter above the bottom was kept within the interval 35 cm/s to 55 cm/s giving a Shield parameter from 0.10 to 0.23 in which θ is defined as:

$$\theta = \frac{U_f^2}{g(s-1)d_{50}}$$

where U_f, the friction velocity associated with the far field, is calculated using the Colebrook-White equation.

Three different materials were used for the scour protection: Round stones with a mean diameter (d_{50}) of D_{cover}=10.3 cm with d_{15}=9.0 cm and d_{85}=11.2 cm, The stones were used in one layer with a mean thickness of 7.6 cm; crushed stones with mean diameter of D_{cover}=4.3 cm with d_{15}=3.7 cm and d_{85}=4.9 cm and, the stones were used in one, two and three layers with a mean thickness of 3.2, 6.2 and 9.0 cm, respectively; crushed stones D_{cover}=1.9 cm with d_{15}=1.6 cm and d_{85}=2.8 cm, the stones were used in one and two layers with a mean thickness of 1.8 and 3.3 cm, respectively.

RESULTS

Fixed-Bed Results

The flow around/in the scour protection around the monopile has been investigated using flow visualization and velocity measurements (LDA). The flow visualizations were made by adding blue and green dye at the edge of the scour protection and in between the stones adjacent to the upstream side of the pile. Only one layer of 4 cm stones was used in order not to block the view of the flow near the base bottom and to keep the overall view relatively simple.

The flow visualizations showed that flow pattern around the monopile is very similar to the pattern around an unprotected monopile. The flow around an unprotected pile has been studied extensively and the results are compiled in for example Sumer and Fredsøe (2002). In relation to scour development the most important flow feature is the horseshoe vortex, see for example Baker (1979) and (1985), Niedoroda and Dalton (1982), Dargahi (1989) and Roulund et al. (2005).

The present flow visualization showed that the horseshoe vortex is still the main reason for the removal of sediment close to the upstream side of the pile, see Figure 4: When adding dye at the top of the stones adjacent to the upstream side of the pile, the dye was transported down into the stones and then upstream in between the stones. Around 10 to 15 cm from the upstream edge of the pile and 10 to 15 cm from the upstream edge of the scour protection these two, opposite directed flows met at a separation line. At the separation line they were forced upwards into the main flow and transported away.

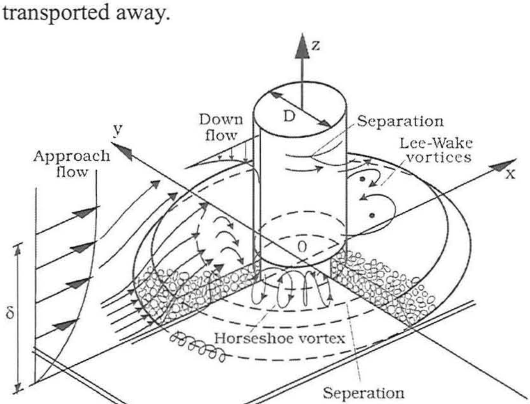

Figure 4 Sketch of the flow around a mono-pile with scour protection.

By adding dye at the upstream edge of the scour protection two important flow patterns were observed: Small horseshoe vortices were generated in front of the protection stones (as sketched in Figure 4) while water was able to flow into the scour protection in the gaps between the stones.

Flow visualizations were made at different position at the side of the pile and downstream of the pile. These flow visualizations showed no important flow features in relation to the sinking of the scour protection. The flow at the side of the pile was dominated by the downstream part of the horseshoe vortex. A flow into the scour protection at the downstream edge of the scour protection was observed, but this flow was weak and it has not been possible to relate it to any important effect in relation to the sinking of the scour protection. The most important flow feature at the downstream side of the cylinder is the vortex shedding, see Figure 4. The live-bed tests showed that the vortex shedding was not causing any significant sinking, however.

Velocity profiles in between the stones have been measured from approximately 1.5 cm above the base bottom to the surface using LDA. The reason for the relatively large distance from the base bottom to the lowest measuring point was that the LDA probe needed to be vertical in order to measure in between the stones. This caused some heavy reflections from the base bottom which made it impossible to measure closer to the bottom with the available equipment.

The velocity profiles upstream of the pile are shown in Figure 5. It is clearly seen that a significant return flow is present in between the stones up to around 10 cm from the edge of the pile. This is consists very well with the results of the flow visualizations.

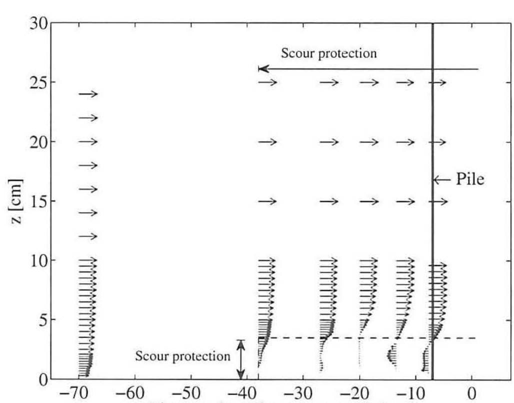

Figure 5 Velocity profiles at different distances to the mono-pile with one layer of 4 cm stones. The undisturbed velocity is 40 cm/s.

As mentioned previously, small horseshoe vortices were observed in front of the protection stones at the upstream side of the scour protection. This will, combined with the inflow in the gaps between the stones, cause edge scour. However, edge scour is not a problem as long as the scour protection is large enough and contain enough material. With the edge scour, the stones will slump down into the scour hole and form a protective slope.

The flow into the scour protection at the downstream side of the pile is very weak and is not able to carry any significant amount of sediment. The sediment bed tests showed a significant deposition of sediment in between the stone in the wake of the pile and only very little or no sinking at all at the downstream edge of the pile, contrary to the case of an unprotected pile, where the vortex shedding is responsible for the scour at the downstream side of the pile, see e.g. Sumer and Fredsøe (2002).

Live-Bed Results

The live-bed tests showed a clear correlation between the sinking of the scour protection, the stone size, the thickness of the scour protection and the pile diameter. The flow visualizations showed that the horseshoe vortex penetrated into the scour protection.

Based on the results of the flow visualizations and the velocity measurements the flow pattern around the pile causing the sinking of the scour protection can be described as follows: The horseshoe vortex caused by the pile penetrates into the scour protection and causes scouring adjacent to the upstream side of the pile. The scoured material is transported by the horseshoe vortex either upstream to the separation line or to the sides. The material will in both cases be deposited in between the stones, relatively far from the pile or, if the horseshoe vortex is strong enough, sucked/winnowed up into to the main body of the flow and transported downstream. The reason for the suction/winnowing of the sand out from the scour protection is a combination of suction by the main flow, as described in Sumer et al. (2001), and the upward directed flow at the separation line between the incoming flow and the horseshoe vortex. The tests have shown that the deposition inside the scour protection is very limited on the upstream side of the pile, and for this reason most of the sediment must be sucked out from the scour protection and transported away. Sumer et al. 2001 used the parameter e/D_{stone} as the non-dimensional parameter for the sinking of an undisturbed protection layer. The process for a scour protection around a pile is in many ways similar to that described above and the parameter e/D_{cover} is also adopted for the present process as well.

The size and strength of the horseshoe vortex is determined by the flow velocity and the pile size. The velocity is indirectly included in the Shields parameter, while the pile diameter is not included in any of the other parameters above. The horseshoe vortex causes the removal of the sediment and a larger pile/horseshoe vortex will, in absolute terms, cause a larger sinking. On the other hand, for a given pile diameter, the larger the ratio D_p/D_{cover}, the larger the penetration of the agitating forces. Therefore the sinking, e_{max}/D_{cover}, should be larger for larger values of D_p/D_{cover}. If the ratio D_p/D_{cover}=0 the situation is the undisturbed protection, Sumer et al. (2001). In this case Sumer et al. (2001) showed that the ratio e_{max}/D_{cover}=0.1 for one layer of stones, in agreement with the trend seen in Figure 6.

Figure 6 shows the non-dimensional sinking relative to the non-dimensional pile size for $0.06<\theta<0.20$. There is a clear trend that the larger the pile diameter, the larger the sinking. This is obviously linked to the horseshoe vortex; the larger the pile diameter, the larger the horseshoe vortex, and the larger the scour underneath the stones, and therefore the larger sinking. The sinking decreases for increasing number of layers. When the number of layers is increased from one to two the sinking is decreased with around a factor of two for D_p/D_{cover} smaller than around 5, however, the effect is much smaller for D_p/D_{cover}=10. There have only been made one test with three layers and considering the scatter of the results with one and two layers it is not clear if the third layer provide any significant extra protection.

Regarding the scatter in the data in Figure 6, this may be attributed to the way in which the stones are laid around the model pile, considering the fact that the stone size in the tests was relatively large.

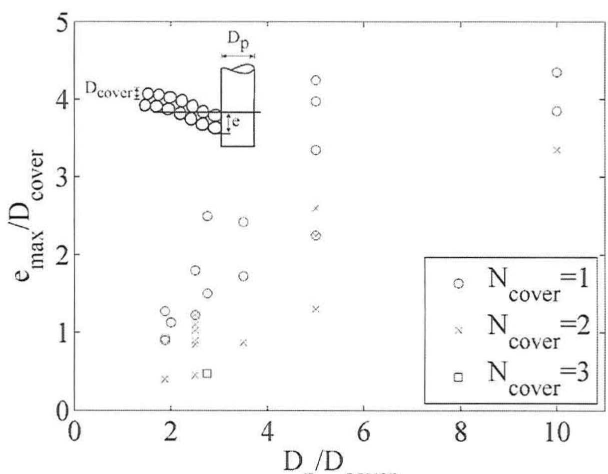

Figure 6 Results of the live-bed tests. The the range of θ is $0.10<\theta<0.23$ and that of h/D_p is $1.5\leq h/D_p\leq 5.1$.

CONCLUSION

The mechanism causing sinking of the scour protection adjacent to the mono-pile has been identified as the horseshoe vortex penetrating into the scour protection. When the horseshoe vortex penetrates into the scour protection it transport the sediment adjacent to the pile upstream, where it is winnowed and transported away by the main flow.

- It is found that a larger pile diameter relative to the size of the protection stones will cause a larger sinking. The maximum sinking is found to be approximately 4 to 4.5 times the diameter of the cover stones in case of one layer of stones and approximately 3 to 3.5 in case of two layers of stones.
- Two layers of stones will decrease the sinking relative to one layer of stones with the same size. For values of D_p/D_{cover} smaller than approximately 5 the sinking seems to be reduced by a factor of two if the number of layers is increase from one to two.

ACKNOWLEDGEMENT

This research was carried out as part of the Statkraft Ocean Energy Research Program, sponsored by Statkraft (www.statkraft.no). The study was partially supported by the Danish Council for Strategic Research (DSF)/Energy and Environment under the program Seabed Wind Farm Interaction (http://sbwi.dhigroup.com, sagsnr. 2104-07-0010) and DHI (www.dhigroup.com). The fixed-bottom experiments and a major part of the live-bed experiments were conducted by MSc Adriana Hudecz. A part of the live-bed experiments were conducted by François Roignant.

REFERENCES

Baker, C.J. (1979). *"The laminar horseshoe vortex"*. J. Fluid Mechanics, vol. 95, part 2, 347-367

Baker C.J. (1985). *"The position of points of maximum and minimum shear stress upstream of cylinders mounted normal to flat plates"*. J. Wind Eng. And Industrial Aerodyn., vol. 18, 263-274

Breusers H.N.C. and Raudkivi A.J. (1991). *"Scouring- Hydraulic design considerations"*, A.A. Balkema.

Chiew, Y.M. and Lim, F.-H. (2000). *"Failure behaivior of riprap layer at bridge piers under live-bed conditions"*. J. Hydraulic Eng. Vol. 126, No. 1, 43-55.

Chiew Y.M. (2002). *"Failiure mechanisme of riprap layer around bridge piers. Proc., First Int. Conf. on Scour of Foundations"*, H.-C. Chen and J.-L. Briaud, eds., Stallion Press, Singapore, Vol. I, 70-92.

Dargahi, B. (1989). *"The turbulent flow field around a circular cylinder"*. Experiments in Fluids, vol. 8, 1-12.

De Vos, Leen (2008). *"Optimisation of scour protection design for monopiles and quantification of wave run-up – Engineering the influence of an offshore wind turbine on local conditions"*. PhD Thesis, Dept. of Civil Engineering, University of Ghent, Ghent, Belgium.

Hoffmanns, G.J.C.M. and Verheij H.J. (1997). *"Scour manual"*. A.A. Balkema.

Lachlan, C.S. and Melvile, B.W. (2001). *"Riprap protection at bridge piers"*. J. Hydraulic Eng. Vol. 127 No. 5, 412-418.

Melville, B.W. and Coleman S.E. (2000). *"Bridge Scour"*. Water Resources Publications, LLC, CO, USA, 550 p.

Niedoroda A.W. and Dalton C. (1982): *"A review of the fluid mechanics of ocean scour"*, Ocean Engineering, vol. 9, No. 2, 150-170.

Roulund A., Sumer B.M., Fredsøe J. and Michelsen J. (2005). *"Numerical and experimental investigation of flow and scour around a circular pile"*, J. Fluid Mech., vol. 534, 351-401.

Sumer, B.M., Cokgor S. and Fredsøe J. (2001). *"Suction of sediment from between armour blocks"*. J. Hydraulic Engineering, ASCE, vol. 127, No. 4, 293-306.

Sumer B.M. and Fredsøe J. (2002). *"The mechanics of scour in the marine environment"*, World Scientific.

Whitehouse R. (1998). *"Scour at marine structures"*. Thomas Telford Publications.

Scour Assessment in Complex Marine Soils – An Evaluation through Case Examples

J.M. Harris[1], M.ASCE, R.J.S. Whitehouse[1] and J. Sutherland[1]

[1]HR Wallingford, Howbery Park, Wallingford, Oxfordshire, OX10 8BA; +44 (0)1491 835381; email: j.harris@hrwallingford.co.uk; r.whitehouse@hrwallingford.co.uk; j.sutherland@hrwallingford.co.uk

ABSTRACT

Scour in cohesionless soils (i.e. sand or gravel) is relatively well understood. The prediction of scour in cohesive or multi-modal soils (i.e. clay, silt, sand/gravel/clay mixtures) is more complex. Typically the scour process is much slower; as a result the effect of scour is very much dependent on the period of time that the structure will remain at the site. This paper describes the application of the Earth Materials approach to estimating scour depth applied to three different case studies. The approach can be applied using information obtained during site investigations but requires good information on soil properties with depth through the seabed. The method relies on previously calibrated formula for stream power at the seabed, which in the original proposed form theoretically allows scouring to continue even beyond the maximum allowable scour depth in some circumstances.

INTRODUCTION

Scour in the marine environment is a physical process related to the movement of seabed sediment by the flow of water away from a structure. The soil conditions are described by geotechnical parameters, therefore, scour is of a geotechnical nature as it relates to the reduction in ground level around a structure.

For scour in non-cohesive soils numerous methods have been proposed. In cohesive or multi-modal soils the scour process may be dependent on not only the physical properties of the soil but also chemical, electrostatic and other properties as well as biological activity at the seabed and predictive methods are less well developed in this area.

Annandale (1995) proposed an approach to estimating the erosion potential of complex soils through the use of the stream power parameter, P, and its relationship to the ability of the soil to resist scour, defined through an erodibility index, K. The erodibility index provides a measure of the *in-situ* strength of the material, whilst the stream power provides a measure of the rate of energy dissipation in the near-bed region expressed by the following relationship:

$$P = f(K) \tag{1}$$

If P exceeds the erosion threshold then scouring will occur. The approach was originally developed for looking at scouring of rock spillways, but the methodology applies equally to marine soils (Chapter 10, Annandale, 2006; Nairn and Anglin, 2002). The erodibility index is defined as:

$$K = M_S K_b K_d J_S \tag{2}$$

Where M_S is the mass strength number; K_b is the block size number; K_d is the discontinuity bond shear strength number and J_S is the relative ground structure number (see Annandale, 2006, for further details). Equation (2) was originally proposed by Kirsten (1982) to characterize how easily earth material can be excavated.

Whilst other methods have been proposed for scour in cohesive soils, it is the approach of Annandale that will be explored further in this paper through the use of available field data. The method has merit in that, theoretically, it can account for changing soil layers and can be applied using typical information obtained during geotechnical field surveys. Three examples will be presented together with a discussion of the results and recommendations on the application of the method.

SCOUR PREDICTION METHODOLOGY

To use the approach of Annandale for determining the potential depth of scour around a structure requires the use of several relationships and assumptions. This may limit the application of the approach to more complex situations unless supported by information from additional studies such as physical modelling, and without information on the soil properties including their variation with depth, this method cannot be applied.

The seabed soil profile is discretised into $n = 1, \ldots, N$ horizontal planes, according to the soil characteristics at each level (derived normally from the bore hole log). Each layer is assigned a required stream power for erosion P_R. Starting at the surface layer ($n = 1$) the stream power at the base of each layer, P_n, is calculated by applying a standard form of reduction profile:

$$P_n = ae^{-b(S/S_{\max})}P_a \qquad (3)$$

Where:

a and b are coefficients obtained by fitting to data;
S_{max} is the maximum scour depth independently determined;
S is the depth of the base of each layer ($0 < S \leq S_{max}$);
S/S_{max} is the relative scour depth; and
P_a is the stream power at the surface in the absence of a structure.

At the seabed surface S = 0, so $P_1 = aP_a$ (for an infinitely thin top layer) so the coefficient a represents the increase in stream power caused by the presence of the seabed structure compared to the no-structure case. If scour is to occur, $aP_a > P_R$. Assuming that the stream power is equivalent to the product of bed shear stress and flow velocity, hence on the open seabed $P_a \equiv \tau U$, and to first order based on potential flow theory the speed local to a circular pile is two times the ambient value, then also to first order the local enhancement to stream power acting on the surface layer of the soil adjacent to the pile is $P_1 = 2^2\tau \times 2U = 8P_a$. The coefficient b denotes the rate of reduction in stream power with depth as layers are removed. Based on fitting of Equation (3) to laboratory data Annandale (2006) gives a = 8.95 and b = 1.92 for circular piles, while for square piles a = 8.42 and b = 1.88. This implies that the increase in bed stream power caused by the presence of square pier is smaller than that caused by a circular one. The values of the leading coefficient a are of similar magnitude to the value of a estimated based on potential flow theory, i.e. 8.

To evaluate Equation (3) there is a requirement to calculate the maximum scour depth, S_{max}. Determination of the maximum scour depth is assumed to be given by the HEC18 methodology (Richardson and Davis, 2001). This expression is based on an envelope curve that embraces known data of scour depth around bridge piers. The approach is generally considered to be conservative.

$$S_{\max} = 2.0K_1K_2K_3K_4h_0F_r^{0.43}\left(\frac{D_p}{h_0}\right)^{0.65} \quad \textbf{(4)}$$

Where D_p is the pile diameter (m); h_0 is the flow depth (m); K_1 is a correction factor for pile nose shape; K_2 is a correction factor for angle of attack of flow; K_3 is a correction factor for bed condition; K_4 is a correction factor for size of bed material and F_r is the Froude number.

Having determined S_{max} it is possible to calculate the dimensionless scour depth as a function of the lower depth of each sediment layer. Following Annandale's derivation the relative stream power (P/P_a) as a function of depth can be calculated using Equation (3) with the result from Equation (4) inserted.

At the maximum scour depth (layer N) the relative scour $S/S_{max} = 1$ so $P_N = ae^{-b}P_a$ which is by inspection smaller than at the seabed. For a circular pile $P_N/P_a = 8.95\ e^{-1.92} = 1.3$. It follows that if $1.3\ Pa > P_R$ then erosion should occur at a depth of S_{max}. For example, if near a circular pile $P_R = 1.2P_a$, then at the surface $P_1 = 8.95Pa = 7.5P_R$ and at the maximum scour depth $P_N = 1.3P_a = 1.1P_R$. In this case we would expect scour to occur at the maximum scour depth, which is unrealistic. Whilst it appears that Annandale must have calibrated with results *for* $P_R > 1.3P_a$ the method is used as published in the current assessment, although an alternative form of Equation (3) that avoids this problem has been derived but is not reported here (paper in preparation).

CASE EXAMPLES

Several examples will be presented for foundations in the marine environment which use realistic input data for metocean and soil conditions. The calculations have been undertaken for a range of site specific circular monopile foundations varying in diameter from 4 m to 4.75 m.

Example 1:

This example is for a sand site and has been used as a 'control' for the methodology. The site in which the monopile is located comprises fine to medium sand with a median grain size, d_{50}, of around 0.2 mm to 0.4 mm. The mean spring tidal range at the site is 2.1 m and the tidal current velocities range from 1 m/s to 1.25 m/s. The significant wave heights that can be expected here are between 0.5 m and 1 m for 10% of the year and 5 m for 1:1 year waves. Waves with a 50 year return period, however, are known to reach 7 m. A peak wave period of 8.2 s was adopted.

Comparing the predictions using the Annandale approach with two commonly applied methods, namely Breusers *et al.* (1977) and Richardson and Davis (2001) (Table 1), the predictions using Annandale and Richardson and Davis give values which would sit either side of the line of exact fit. The method of Breusers *et al.* with a multiplier of 1.5 gives the largest prediction, with some correction for shallow water reducing the predicted scour. However, there is a time-element to the scouring in that the hydrodynamic conditions from a tidal perspective alone are continually changing and it is uncertain as to what conditions had occurred or were persisting at the time of the scour survey. The methods give a range of predicted depths. The approach of Annandale has been applied to a combined wave and current case as well as a current alone case. For all conditions $S/S_{max} = 1$ is assumed to be the limiting condition and, therefore, in the limit, the results from the Annandale method correspond to the predictions of Richardson and Davis (2001).

Table 1: Comparison of scour predictors against measured data.

Methodolgy	Normalised Scour depth	
	$S_{predicted}/D$	$S_{measured}/D$
Richardson and Davis (2001) – typical conditions	0.97	1.20
Richardson and Davis (2001) – extreme conditions	1.30	1.20
Breusers *et al*. (1977) – 1.5 multiplier	1.46	1.20
Annandale (2006) – typical conditions (currents only)	0.97	1.20
Annandale (2006) – extreme conditions (currents only)	1.30	1.20

Example 2:

The example relates to an area of sandwaves on, and in proximity to, a sandbank with a maximum height of around 5 m. The sandbank and sandwaves consist of fine to medium sands deposited in the Holocene period and are found at a depth of between 0 m to 3 m, approximately. Borehole information indicates that the sediments underlying the sandbank to the east and the sandwave features to the west of the site consist of a soft to firm organic rich clay and these deposits are found at a depth of between 3 m to 5 m. The surficial sediments tend to be fine to medium sands (0.125 mm to 0.500 mm) with low organic carbon content due to the relatively strong current speeds that lead to a winnowing out of the fine grained sedimentary and organic particles. From a benthic study of the site the median sediment characteristics have been indicated to be 0.578 mm with a maximum and minimum grain size of 0.642 mm and 0.470 mm, respectively. This suggests the surficial sediments to be coarse grade rather than fine to medium grade. In the present example median grain sizes of between 0.125 mm and 0.200 mm have been used at BH4 and BH8, respectively, based on the sediment sample analysis.

The tides are semi-diurnal and residual surface tidal currents run approximately parallel to the local coastline. The 50 year design conditions indicate the local depth-averaged current for both tidal and wind-driven currents is 1.3 m/s, whilst the wave conditions are a significant wave height of 7.7 m and a mean wave period of 9.7 s.

Borehole data at two locations, BH4 and BH8 show the soil profiles to a depth of 20 m below the seabed to consist of fine and medium sand with a dense or very dense structure (Figure 1). From analysis of the soil test data a clay layer is interpreted at between 2 m and 2.9 m at BH4, although this does not appear in the borehole record. The undrained shear strength, S_u, within this stratum is calculated to be 20 kPa.

From bathymetric survey measurements the scour depth at the monopile associated to BH4 was 2.9 m deep after 301 days from installation of the foundation. At BH8 the scour hole was 2.1 m deep after 270 days from the installation of the associated monopile. The interpreted clay layer at BH4 inhibits the scour development in the prediction to the start of the clay layer, at 2 m below the existing seabed level (Figure 2). From the bathymetric survey data scouring at this location appears to have eroded through the clay layer.

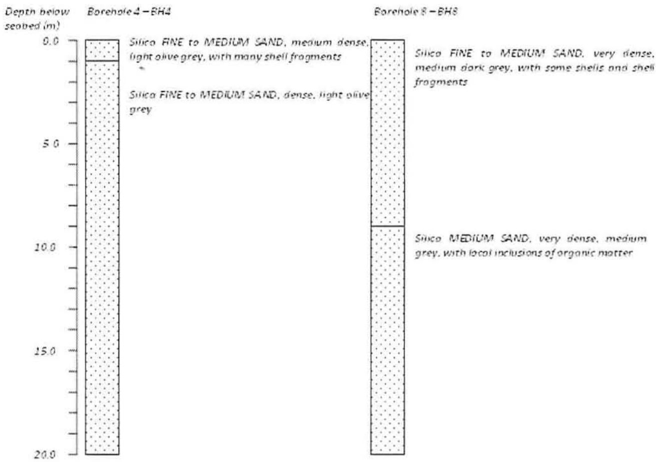

Figures 1: Borehole data for Example 2.

An assessment of the scour depth at this location has also been made by applying the SRICOS method (Briaud *et al.*, 1999). This approach was developed to predict scour at a cylindrical pier under steady flows, uniform soils and a water depth greater than two times the pier diameter.

$$S_C = 0.00018\,\mathrm{Re}^{0.635} \quad \textbf{(5)}$$

Where:

$$\mathrm{Re} = \frac{D_p U_c}{\nu} \quad \textbf{(6)}$$

Re is the Reynolds number, U_c is the depth-averaged current speed, and ν is the kinematic viscosity of water. The formula is independent of soil properties and is considered to represent the maximum possible depth of scour in clay. Therefore, the maximum scour depth is governed by the pile diameter, current speed and kinematic viscosity of the water and it would be expected that as the current velocity increases so the erosive capacity of the flow will also increase.

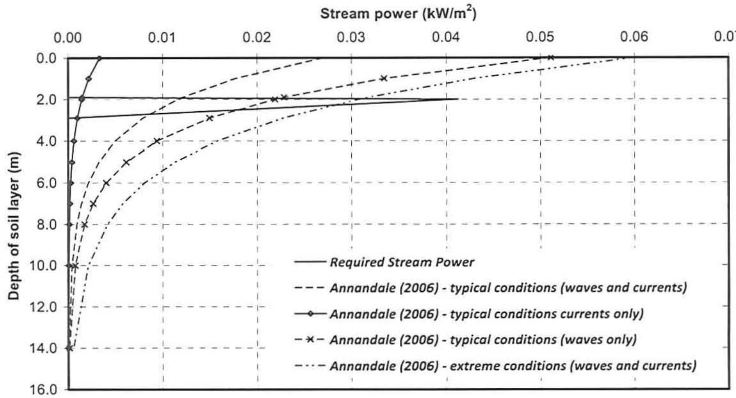

Figure 2. **Plot showing the extent of scour for typical and extreme hydrodynamic conditions at BH4.**

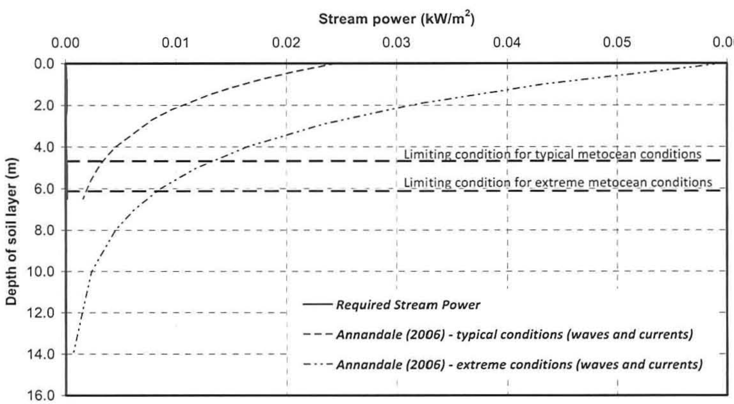

Figure 3. **Plot showing the extent of scour for typical and extreme hydrodynamic conditions at BH8 (Example 2).**

If we assume that the clay layer at BH4 exists from the seabed level downwards, the maximum predicted scour depth using this approach is between around 2 m to 3 m depending on the hydrodynamic conditions, whereas the using the Earth Materials approach, the stream power is not of sufficient magnitude to get through the clay layer limiting the scour to 2 m or less.

The prediction for scour development at BH8 using the method of Annandale corresponds to the limiting condition of S/S_{max} = 1 (Figure 3). From measurements at the site the scour depth after 270 days is around 2.1 m suggesting either infilling has occurred or that the scour depth is being limited by the geotechnical conditions. However, without knowledge of the metocean conditions existing at the time of the survey, as well as the time history of the metocean conditions that have occurred since installation of the foundation, it is unclear as to whether the scour hole as measured can be associated with typical hydrodynamic conditions at the site.

Example 3:

This example site comprises mainly sand with concretions overlying tillite and clays, and an area where exposures of tillite and clays dominate and the surface sand becomes patchy. The depth of surface sediment reaches 10 m in some parts but this depth includes bedded muddy sands as well as the surface layer of sand.

Geophysical surveys including borehole sampling revealed the bed material at the western side of the site consists of medium dense becoming very dense brown silty fine sand with occasional shell fragments. This layer extends to 10.8 m beneath the surface, with patches of very dense sand and occasional other material, such as coal fragments and quartz granite fine to coarse gravel. The sand at this location is very fine at 1.75 m below the surface, with a significant fraction smaller than 0.06 mm (the boundary between sand and silt). The sand increases in size on going down through the layer. Beneath the sandy layer is a thick layer of stiff, becoming very stiff, slightly gravelly clay with occasional cobbles.

At borehole (BH8 – whilst this is the same nomenclature as in Example 2 it is a different site) the top 3 m of seabed consists of very silty, fine sand. Beneath the top layer of sand is a 6 m deep layer of slightly laminated, slightly sandy clay. Within the clay dominant area of the site some of the borehole data shows a sand veneer extending only around 0.1 m below the surface. Beneath this veneer of sand is another 0.1 m deep layer of very gravelly, sandy clay and underlying this layer is a 6.1 m thick layer, also of very gravelly, sandy clay. Underneath this are alternate layers of sand and clay.

The rectilinear tidal currents over the site have peak spring and neap current speeds reported to be 0.67 m/s and 0.34 m/s. The 1-year return period significant wave height, H_s, is 4.8 m at the offshore edge of the site, with a corresponding peak wave period of T_p = 9.8 s. Based on the analysis of wave statistics a significant wave height of 0.5 m is only exceeded 25% of the time.

Prediction of scouring at BH8 using the method of Annandale gives a scour depth of 2.3 m, approximately, for normal hydrodynamic conditions (Figure 4). From bathymetric surveys of the site the scour depths in the vicinity of the borehole have been shown to vary over time but are typically in the range of 1 m to 3 m (Figure 5). Figure 5 also shows a general change in seabed scour depth over time due to bed erosion and infilling. The clay layer acts to inhibit scouring beneath the upper sand layer as discussed previously by Whitehouse *et al.* (2008).

DISCUSSION

Three case examples have been presented demonstrating the application of the Earth Materials approach of Annandale (1995; 2006). The studies represent first order assessments supported with some post-construction surveys of scouring. Uncertainty in scour prediction and assessment arises from a number of factors. These include metocean and soils data, the modelling methods applied, details of the structure and the influence of the foundation installation phase. Methods based on purely sand soils cannot be applied with certainty at those sites where a range of soils are found as they are conservative predicting a maximum scour depth (e.g. Equation (4)), which of course may be appropriate for design.

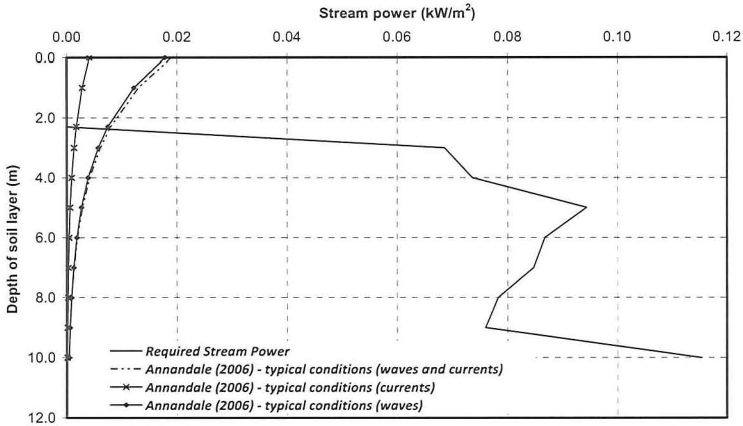

Figure 4. Plot showing the extent of scour for typical hydrodynamic conditions at BH8 – Example 3.

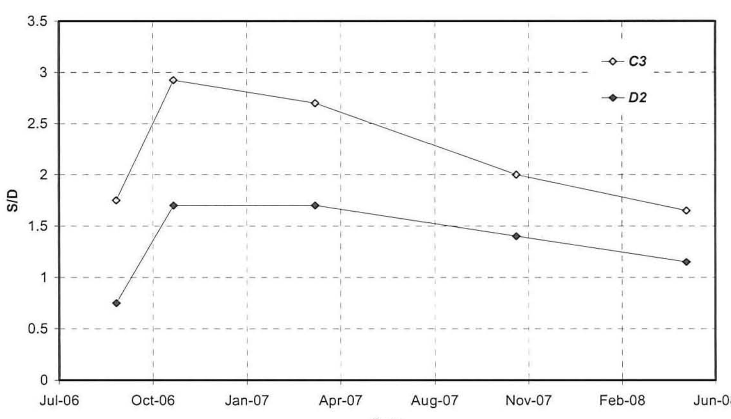

Figure 5: Variation of scour depth over time at two foundation positions.

The method of Annandale has great potential for predicting scour in complex marine soils, but to reduce uncertainty in its application requires further detailed testing for a wide range of conditions. For scour assessments in general it is very important to know the surficial soil characteristics and data analysis starting from 1 m below the seabed or deeper in a foundation site investigation may not be representative of the surface sediment properties required for a scour assessment. However, knowledge of the sediment properties below the bed level will be important for predicting scour development with depth through the seabed. The quality of assessment will depend on the number N and thickness of soil layers distinguished and characterised within the depth range to at least S_{max} (Equation (4)). Geotechnical parameters such as SPT blows may be accurate to within ± 25 %, whilst for clays there will be some uncertainty in the values typically obtained as part of site investigations for bed density and vane shear strength, with accuracy in the order of ± 5%. Uncertainty will also arise from spatial variability within and between samples at a given site, and temporal variation in sediment properties. The influence of layering in sandy and silty soils or the presence of a veneer of mobile sediment overlying, for example, stiff clay can be taken into account in the scour assessment if detailed site survey data is available. The rate of erosion has not been evaluated and hence the prediction is of potential depth.

CONCLUSIONS

Scour is a physical process related to the movement of sediment by the flow of water away from a structure. The soil conditions are described by geotechnical parameters, therefore, scour is of a geotechnical nature as it relates to the reduction in ground level around a structure. Soil mechanics testing provides workable definitions of the complete spectrum of soil types from pure cohesionless sands to clays.

The approach of Annandale (1995; 2006) has been used to assess the scour potential at three contrasting offshore locations. The approach allows for the physical properties of the soil to be considered and although the method does not directly take into account the chemical properties of the material, the mass strength number, M_S, represents the relative influence of chemical bonding properties of the soil through the unconfined compressive strength. The method represents an engineering methodology that can be applied using information obtained during geotechnical site investigations. Key considerations for application include:

- The requirement for good information on the soil properties with depth through the seabed, including grain size distributions, density, undrained shear strength, internal angle of friction, etc from the seabed surface to the depth (at least) of S_{max}.
- Knowledge of the metocean conditions for both typical and extreme events.

Furthermore:

- The method relies on previously calibrated formula for the stream power at the seabed P_l and shape of the curve P_n with depth in the soil. The curve retains values of $P_N = 1.3P_a$ at the base of the scour hole at depth S_{max} and theoretically scouring may continue (if $P_R < 1.3P_a$). Hence an alternative approach is to solve for $P_R = P_N$ at $S/S_{max} = 1$, which is being considered by the authors elsewhere (paper in preparation).
- The determination of the development of scour through time in complex marine soils requires further research, especially for soils with multi-modal grading distributions and with distinct layering.

- It is important to determine any adjustment to soil properties that might occur during foundation installation that could affect resistance to scouring.

REFERENCES

Annandale, G.W. (1995). Erodibility. Journal of Hydraulic Research, 33 (4), 471-494.

Annandale, G.W. (2006). Scour Technology. Mechanics and Engineering Practice. McGraw-Hill.

Breusers, H.N.C, Nicollet, G. and Shen, H.W. (1977). Local scour around cylindrical piers. *J. of Hydraulic Res.*, IAHR, Vol 15, No. 3, pp. 211 252.

Briaud, J-L., Ting, F., Chen, H.C., Gudavalli, S.R., Perugu, S., and Wei, G. (1999). SRICOS: Prediction of scour rate in cohesive soils at bridge piers. J. Geotechnical Engng., ASCE, Vol. 125, pp. 237-246.

Kirsten, H.A.D. (1982). A classification system for excavation in natural materials. *The Civil Engineer in South Africa*, July, pp. 292 – 308.

Nairn, R.B. and Anglin, C.D. (2002). Confederation Bridge – New scour design methodology for complex materials. *Proceedings First International Conference on Scour of Foundations*, Texas A&M University, College Station, TX, pp. 978-992.

Richardson, E.V. and Davis, S.R. (2001). *Evaluating Scour at Bridges*. Hydr. Engng. Circular No. 18, US Department of Transport, Federal Highway Administration, Pub. No. FHWA NHI 01-001.

Sumer, B.M. and Fredsøe, J. (2002). *The Mechanics of Scour in the Marine Environment*. Advanced Series on Ocean Engng., Vol. 17, World Scientific, Singapore. xiii + 536 pp.

Whitehouse, R., Harris, J., Sutherland, J. and Rees, J. (2008). An assessment of field data for scour at offshore wind turbine foundations. *Proceedings Fourth International Conference on Scour and Erosion*, Tokyo, Japan, Paper B-13, pp. 329-335.

Scour Reduction by Collars Around Offshore Monopiles

B. de Sonneville[1], D. Rudolph[2] and T.C. Raaijmakers[3]

[1]Deltares | Delft Hydraulics, Rotterdamseweg 185, P.O. Box 177, 2600 MH Delft, The Netherlands; e-mail:ben.desonneville@deltares.nl
[2]Deltares | Delft Hydraulics, Rotterdamseweg 185, P.O. Box 177, 2600 MH Delft, The Netherlands; e-mail:daniel.rudolph@deltares.nl
[3]Deltares | Delft Hydraulics, Rotterdamseweg 185, P.O. Box 177, 2600 MH Delft, The Netherlands; e-mail:tim.raaijmakers@deltares.nl

Excessive scour is a threat to the stability of monopile foundations, e.g. in offshore windparks. Particularly in shallow waters with strong tidal currents such as the North Sea, protection against excessive scouring is required. Commonly applied scour protection consists of loose rock. Little is known about alternative scour protection measures. One of the alternatives is to use a collar installed around the base of the monopile at seabed level. Indicative laboratory experiments were conducted to investigate whether collars reduce pile scouring under combined current and waves. This paper summarizes the experimental set-up, monitoring techniques, test program and results of the conducted experiments. The analysis focused on the equilibrium scour depth and the rate of scour development. The results showed that collars prevented pile scour under currents. Under extreme storm conditions scour occurred, but with a significant time delay, at a lower rate and a reduced equilibrium scour depth.

INTRODUCTION

Global climate change and the related endeavour of many European governments to stimulate sustainable energy generation have drawn the attention of politics and industry to offshore wind park development. Wind turbine foundations usually consist of monopiles, which are equipped with scour protection because excessive scour can threaten their stability and affect their resonance frequency. The commonly applied scour protection consists of several rock layers.

In recent years, several alternatives have been proposed in order to control scour at piles. They are generally characterized as either altering the flow (e.g. splitter plates, slots, vanes, helical wires) or armouring the seabed (e.g. gravel bags, block matrasses, tetra pods). One of the alternatives might be to use a pre-fabricated collar installed around the base of the monopile at seabed level. The idea of such a collar under current attack is to armour the seabed by preventing downflow and horseshoe vortex development from reaching the seabed. Under waves, the collar is expected to limit wave-induced vortices and turbulence from reaching the seabed.

Previous studies on the scour reduction of collars mainly focused on current-induced scour around bridge piers (e.g. Kumar, 1999). According to these studies, collars can be particularly effective with collar widths larger than 0.5 times the pile diameter when placed close to the bed (see Figure 1 for definitions). A more recent study (Simon et al., 2009) investigated the effect of multiple discs installed at the base of a monopile on current-induced scour with beneficial results for collar widths larger than one pile diameter. Research performed for a comparative concept (cylindrical piles with cone shaped footings) indicated a 50-80% reduction in scour depth compared to a single pile (Rudolph and Raaijmakers, 2007).

To the authors' knowledge, to date there has been no study of the performance of collars under forcing by a combination of a current and waves, as typical in the offshore environment, and the effect of a collar on the time scale of the scour development. The aim of the study presented here is to focus on both aspects. The study was based on indicative laboratory experiments. This paper describes the conducted laboratory experiments (sections 2 and 3), analysis of the results (section 4), conclusions (section 5) and a discussion (section 6).

SETUP OF LABORATORY EXPERIMENTS

Until a few years ago, one of the major shortcomings of laboratory experiments in a wave basin was that scour development was not visible during test execution because of the turbidity of water at high sediment concentrations. Scour hole inspection required drainage of the wave basin. Since this process takes relatively long (several hours, due to the low permeability of the fine sand in the basin), it was not feasible to monitor scour development without time-consuming drainings of the basin.

In 2007, a scour monitoring technique was developed, based on installing a rotating downward facing digital camera with an inclined mirror inside a transparent model during a test (Raaijmakers and Rudolph, 2008). Recently, this technique was innovated by equipping the camera with a fish-eye lens (see Figure 2). High frequency recording of images, combined with automatic image processing software, currently allows for continuous 360° monitoring of the scour development during each test. On each image the interface between water and seabed is detected automatically based on the colour gradient, and converted to a scour depth using calibration functions. This makes it possible to observe whether equilibrium was reached, at which location around the pile maximum scour depths occurred and at which rate the scour developed.

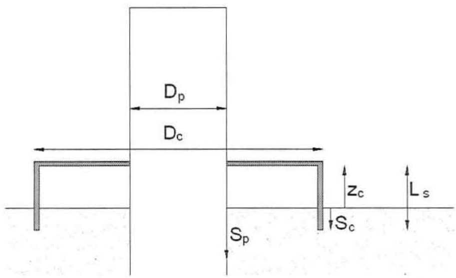

Figure 1 Schematic overview of the pile, collar and skirt setup and definitions.

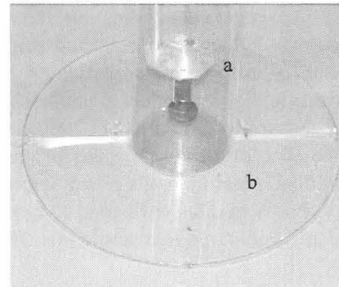

Figure 2 Design of system showing the camera mounted inside the transparent pile (a) and the transparent collar (b).

In the experiment setup, four transparent circular piles with a diameter of 200mm were equipped with the above described camera system and mounted at the bottom of the facility. During each test, one pile was left unprotected, while at the other three piles different configurations of transparent collars were installed. The solid collar discs, installed at a fixed vertical level, had a thickness of 10mm with outer diameters ranging from 2-3 times the pile diameter ($2D_p$ to $3D_p$ – see Figure 1). In some cases, a skirt was attached to the outer diameter of the collar. All tests were performed in Deltares' Scheldt basin (30m x 14m - see Figure 3), which is equipped with a wave generator, several pumps to generate a cross-flow of up to $2m^3/s$ and a bed of fine, non-cohesive sediment (d_{50}=130μm). Five wave height meters and five electromagnetic current velocity meters were installed at the outer edges of the test section.

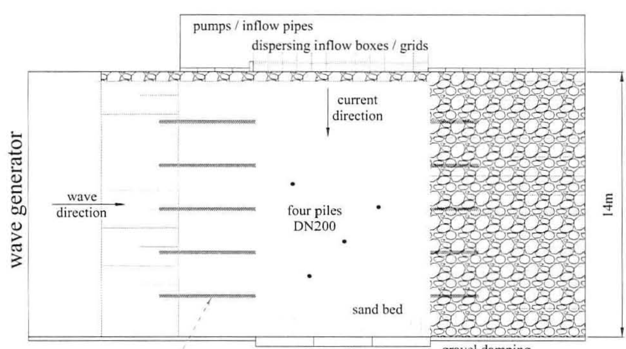

Figure 3 Overview of Scheldt Basin with wave generator at the left, current inflow from above, wave guidance walls and test section in the middle, wave spending beach at the right and outflow weirs at the bottom.

The test programme comprised six tests (see Table 1). The test conditions were guided by typical (storm) conditions occurring at the North Sea, scaled with the Froude criterion with a scale factor of 1:20. Due to limited water depth in the facility, however, for the water depth a distorted Froude scaling was applied. The first test represented a current-only condition, with a flow velocity of about 0.30m/s. Tests 2-6 comprised storm conditions with a significant wave height of about 0.27m and a peak wave period of 2.3 or 3.0s.

RESULTS OF LABORATORY EXPERIMENTS

(1) Introduction

After all tests, the measured significant wave heights, peak wave periods and current velocities were processed and spatially interpolated to the locations of the structures in the basin. The scour development at each of the piles was processed from the camera images with the system described above (see Figure 4).

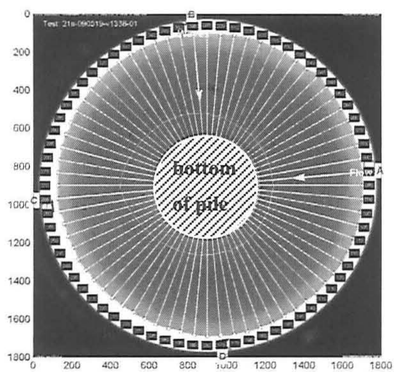

Figure 4a Camera image taken from inside pile (looking downward) at start of test 2a. The dark area around the bottom of the pile indicates the penetration of the pile in the sand. No scour has occurred yet.

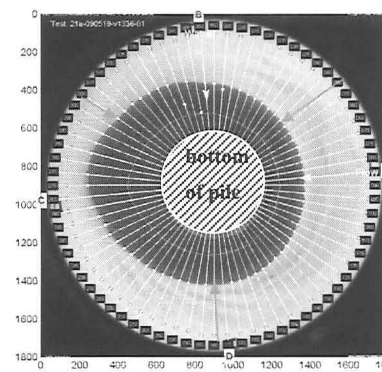

Figure 4b Camera image taken 13 minutes into the test. Scour has occurred, indicated by red arrows. The white dots show the automatically detected interface between sand and water.

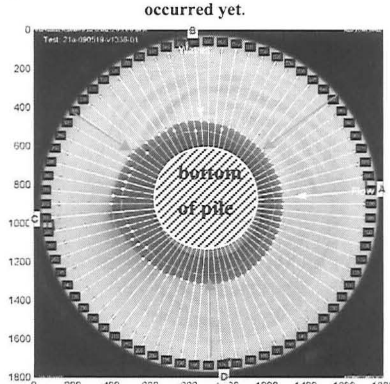

Figure 4c Camera image taken 33 minutes into the test. Additional scouring still occurs, although at a slower rate than at the start of the test.

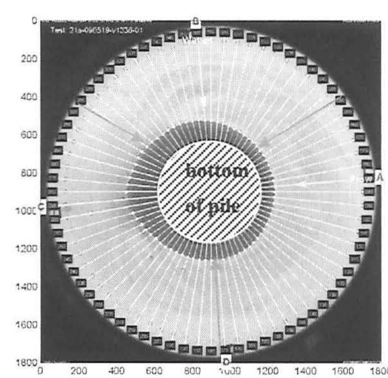

Figure 4d Camera image taken at the end of the test (after about 100 minutes), when the scour depth approaches equilibrium.

In the following analysis the maximum pile scour at the structure (S_p - see Figure 1) is considered, and not the edge scour hole that occurs at the edge of the collar (S_c). Scour at the pile is assumed the most relevant threat for the stability and resonance frequency of offshore monopiles.

According to a commonly adopted approach (e.g. Hoffmans and Verheij 1997, Whitehouse, 1998 and Sumer and Fredsøe, 2002), scour development can be described by an exponential function. In this function, the timescale of scouring is described by the characteristic time (T_{char} - when 63% of the equilibrium scour depth has been reached). We adapted this function to include a delay before scouring starts (t_0), related to the scour protection provided by the collar:

$$\frac{S(t)}{S_{eq}} = 1 - \exp\left(-\frac{t_0 + t}{T_{char}} \right)$$

For each test and each of the four piles, T_{char} and t_0 were determined by fitting this function to the measured data. The function appeared to fit the data rather well (see Figure 5). This confirms the suitability of the assumed exponential function.

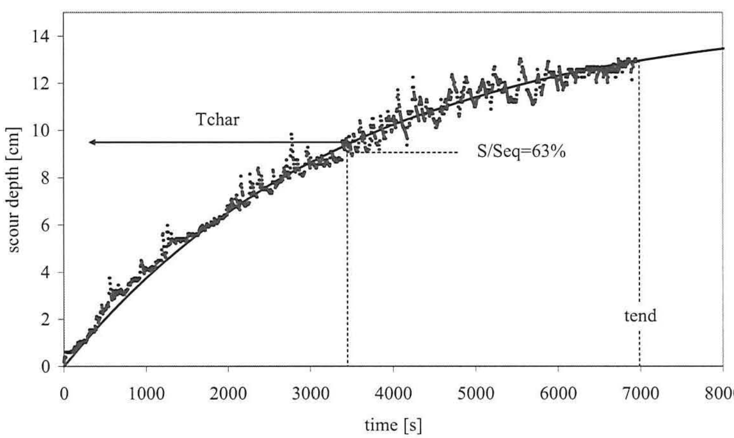

Figure 5 Example of time scale fit (test 1d) at the upstream side of the pile perimeter.

(2) Test results overview

Table 1 shows the results of the six performed tests. The piles are indicated by letters 'a' to'd'. In test 1, 2 and 5 pile 'a' represented the unprotected pile. Test 6 comprised a single pile. In some cases the scour data was not sufficient to provide a reasonable fit for the scour development, which does not mean that no scour occurred (see scour parameters marked 'n/a').

Table 1: Test results showing the collar specifications, the processed measured hydrodynamics and the processed scour development.

test id.	collar			hydrodynamics								scour		
	D_c [m]	L_{skirt} [m]	z_c [m]	h_w [m]	H_s [m]	T_p [s]	u_c [m/s]	t_{end} [min]	U_{bed} [m/s]	KC [-]	U_{rel} [-]	$S_{eq;p}$ [m]	t_0 [s]	T_{char} [s]
1a	0.00	0.00	0.00	0.75	0.000	0.00	0.28	120	0.000	0.0	0.00	0.16	0	3500
1b	0.40	0.00	0.00	0.75	0.000	0.00	0.28	120	0.000	0.0	0.00	0.00	n/a	n/a
1c	0.50	0.00	0.00	0.75	0.000	0.00	0.29	120	0.000	0.0	0.00	0.00	n/a	n/a
1d	0.60	0.00	0.00	0.75	0.000	0.00	0.29	120	0.000	0.0	0.00	0.00	n/a	n/a
2a	0.00	0.00	0.00	0.75	0.269	3.08	0.25	100	0.486	7.5	0.34	0.15	0	1300
2b	0.40	0.00	0.00	0.75	0.280	3.06	0.27	100	0.503	7.7	0.35	n/a	3000	n/a
2c	0.50	0.00	0.00	0.75	0.267	3.00	0.29	100	0.477	7.2	0.37	n/a	3600	n/a
2d	0.60	0.00	0.00	0.75	0.254	2.95	0.30	100	0.450	6.6	0.40	n/a	3400	n/a
3a	0.40	0.04	0.00	0.75	0.283	2.93	0.28	60	0.497	7.3	0.36	0.00	n/a	n/a
3b	0.50	0.04	0.00	0.75	0.273	2.96	0.29	60	0.482	7.1	0.37	0.00	n/a	n/a
3c	0.60	0.00	0.10	0.75	0.262	2.99	0.28	60	0.467	7.0	0.38	0.15	200	400
3d	0.60	0.04	0.00	0.75	0.270	2.94	0.27	60	0.476	7.0	0.36	0.00	n/a	n/a
4a	0.40	0.04	0.00	0.75	0.286	3.10	0.28	120	0.515	8.0	0.35	n/a	5000	n/a
4b	0.50	0.04	0.00	0.75	0.276	3.03	0.29	120	0.493	7.5	0.37	n/a	2000	n/a
4c	0.60	0.04	0.04	0.75	0.266	2.95	0.28	120	0.471	7.0	0.38	0.21	0	2500
4d	0.60	0.04	0.04	0.75	0.271	2.99	0.28	120	0.483	7.2	0.36	0.20	0	3000
5a	0.00	0.00	0.00	0.75	0.276	2.40	0.20	120	0.432	5.2	0.32	0.09	400	1800
5b	0.40	0.04	0.00	0.75	0.280	2.31	0.20	120	0.427	4.9	0.32	0.00	n/a	n/a
5c	0.60	0.00	0.00	0.75	0.273	2.33	0.20	120	0.418	4.9	0.32	0.00	n/a	n/a
5d	0.60	0.04	0.00	0.75	0.265	2.34	0.20	120	0.410	4.8	0.32	0.00	n/a	n/a
6	0.60	0.00	0.00	0.75	0.265	3.00	0.31	330	0.473	7.1	0.39	0.10	6000	5500

ANALYSIS OF RESULTS

(1) Governing processes

Scour around a slender cylindrical pile is governed by three hydrodynamic phenomena (Sumer and Freds¢e, 2002):

- a horseshoe vortex upstream of the pile,
- vortex shedding at the downstream side of the pile and
- streamline contraction

The horseshoe vortex is the dominant phenomenon in case of current-only. As the current encounters the pile, pressure gradients drive it downward around the pile and scour occurs as result of a locally enhanced sediment transport gradient. The size of the horseshoe vortex and consequently the scour depth is mainly determined by the separation distance of the bed boundary layer of the upstream flow. The separation distance is typically in the order of the pile diameter.

In case of waves, the dominating phenomenon is vortex shedding. Each shed vortex sweeps up sediment while it is transported downstream, causing a net increase in scour depth each half wave period. The intensity of vortex shedding depends on the wave-induced water motion at the seabed relative to the pile diameter. This ratio is typically defined as the Keulegan-Carpenter number:

$$KC = \frac{u_{bed} \cdot T_p}{D}$$

in which KC = Keulegan-Carpenter number, u_{bed} = amplitude of undisturbed

bed orbital velocity (based on the significant wave height), T_p = peak wave period and D = pile diameter.

In combined current and waves, the relative velocity is often used to indicate whether the current action or the wave action is dominant:

$$U_{rel} = \frac{u_c}{u_c + u_{bed}}$$

in which U_{rel} = relative flow velocity and u_c = depth-averaged current velocity

(2) Scour at unprotected pile

A significant amount of scouring ($0.8D_p$) occurred at the unprotected pile under the current-only condition (test 1a). The scour was distributed relatively symmetrically around the pile perimeter with a maximum at the upstream side and a minimum at the downstream side (see Figure 6). The characteristic time of test 1a (3500s) indicates that at the end of the test (7200s) the equilibrium scour depth was almost reached. Although the scouring was significant, it was well below the rule of thumb often used in literature, independent on the current velocity: $1.3D_p$ (Sumer and Fredsøe, 2002), and the scour prediction computed with the formula of Sheppard (2006), which is dependent on the current velocity: coincidentally also $1.3D_p$ for test 1a. A possible reason is that the current velocity of test 1a corresponds with a hydraulic regime between the clear-water scour peak and the live-bed scour peak, for which slightly lower scour depths were previously observed by various researchers, e.g. Sumer and Fredsøe (2002). This is not accounted for in the formulae.

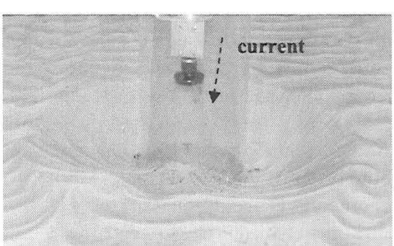

Figure 6 Scour at unprotected pile (test 1a - current-only).

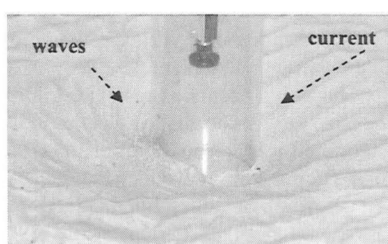

Figure 7 Scour at unprotected pile (test 2a-wave-dominated).

Under combined current and waves (KC ≈ 7), a more or less similar equilibrium scour depth occurred (test 2a) as in the current-only test (test 1a). The extent of the scour hole was slightly less distinct, probably because of enhanced turbulence (see Figure 7). When compared to recent formulae on scour at unprotected circular piles under waves (Raaijmakers and Rudolph, 2008) the scour depth and scour development were in the range of predicted values.

(4) Effect of collar in current

The effectiveness of collars was considered by comparing the scour depth at the unprotected pile with the pile scour depth at the piles protected by collars. Test 1b-d demonstrate that collars are effective under current-only conditions (see Figure 8-9). As opposed to the unprotected pile, no pile scour occurred at the piles protected by collars. Limited edge scour holes (in the order of a few cm) were observed downstream around the edges of the collar (as found in Kumar et al, 1999). This indicates that the scouring is effectively shifted away from the pile and occurs in a zone where the horseshoe vortex is significantly weaker.

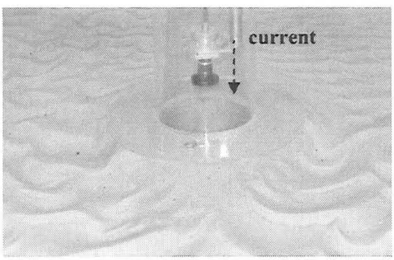

Figure 8 Edge scour at pile protected by smallest collar (test 1b - current-only).

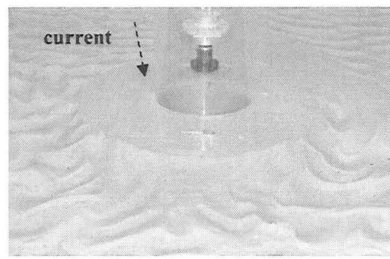

Figure 9 Edge scour at pile protected by largest collar (test 1d - current-only).

(5) Effect of collar in combined waves and current

Under combined current and wave conditions (tests 2-6) collars also proved effective. Although in some cases pile scouring was not prevented completely, in all cases it was significantly delayed and reduced in depth. The general scour pattern at the end of the tests was characterised by a shallow wide depression around the edges of the collars (see Figure 10). This indicates that the scour development was not governed by the horseshoe vortex, but by wave-induced vortex shedding and turbulence. In test 3 collars with skirts were installed. With skirts, in test 3, the delay was sufficiently long to prevent undermining (compare Figure 10 with Figure 11).

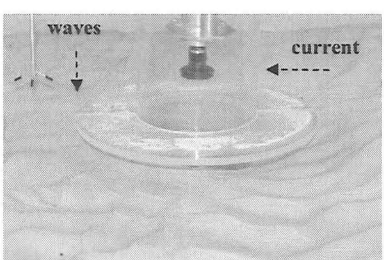

Figure 10 Scour at pile protected by smallest collar (test 2b - wave-dominated).

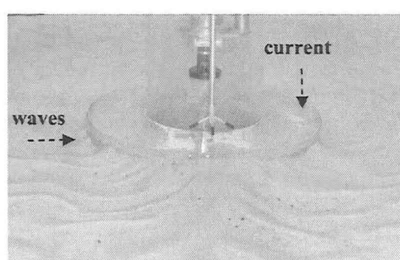

Figure 11 Scour at pile protected by largest collar with skirt (test 3a - wave-dominated).

Analysis of the scour development of test 2 revealed that under combined current and wave conditions, after a significant time delay, pile scour occurred at the piles protected by collars (see Figure 12). Two phases were distinguished: during the first phase the collar effectively protected the bed near the pile against wave-induced shed vortices while the edge scour depression grew. In the second phase, the edge scour depression presumably reached a depth at which the vortices were able to protrude under the collar and sediment was removed from underneath the collar. Test 6, which had a long duration (5.5hrs), confirmed that a 30-35% lower equilibrium scour depth was reached at the end of the test (see Figure 13).

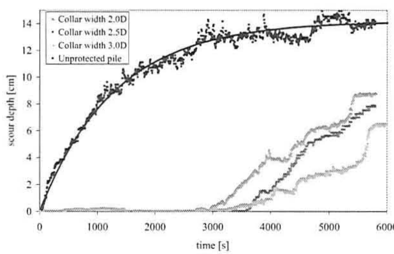

Figure 12 Scour development at unprotected pile (shown in black) and the piles protected by different collar widths (test 2).

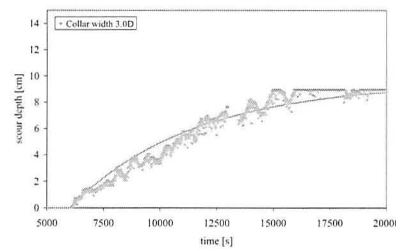

Figure 13 Scour development for pile with a collar width of 3.0D for long duration test. Note that the x-axis starts at 5000s (test 6).

With respect to a collar at a fixed height above the bed, Kumar et al. (1999) report positive results in terms of scour reduction under current-only conditions. In our study, we did not investigate the effect of a higher collar in current-only conditions. Under combined current and wave conditions (test 3c), however, the collar placed at a height of 0.5D above the bed was not effective; the final scour depth was about similar to the unprotected pile, but the rate was even higher (i.e. faster scour development). It appears that a collar at a fixed height is less effective at disrupting the (horizontal) shed vortices under wave-dominated conditions than at disrupting the (predominantly vertical) horseshoe vortex under currents.

Installing skirts at the outer edge of the collars proved to be effective in terms of a larger time delay (test 2b vs. 4a), but when undermining occurred pile scour developed (test 4a,b). Collars with skirts placed at 0.5D above the ground (test 4c-d) proved to have an adverse effect: the final scour depths were even larger than at the unprotected pile under the same conditions (test 2a).

CONCLUSIONS

Laboratory tests were performed to investigate the effectiveness of collars to prevent scour around offshore monopiles. Four transparent piles (200 mm) were placed in the Scheldt basin at Deltares and equipped with cameras with fisheye lenses. At selected piles, collars were installed with different widths, vertical levels and skirt dimensions. Several tests were performed with current-only and combined current and wave conditions. During each test, the scour development around the unprotected pile was derived from the camera images and compared to the pile scour development at the piles protected by collars.

The comparisons indicated that collars are quite effective against scour under currents. Only slight edge scour was observed. Under combined current and wave conditions after a significant time delay scour developed, at a lower rate and with a lower equilibrium scour depth.

Placing the collar at a certain fixed level above the bed significantly increased the scour rate under combined wave and current conditions, compared to the unprotected situation. Installing a skirt at the outer diameter of the collar worked beneficially as pile scouring was delayed, but when the skirt was undermined pile scour occurred. With the collar and skirt at a fixed level above the bed, the pile scour depth became even larger than in the unprotected scenario.

DISCUSSION

The results clearly indicate that collars have potential to provide effective offshore scour protection. Compared to conventional rock dumping, they may have the advantage of a lower material cost and, possibly, a simplified installation procedure. However, the tests also identified aspects that are in need of further investigation. One example is the importance of a good understanding of the time scale of the scour development when collars are present. The tests indicated that the severity and time duration of a storm will ultimately determine whether scour occurs at a collar-protected pile. Recommendations for future research are summarized below:

- Further testing with longer time durations and varying conditions is recommended to better understand the rate of pile scour development when a collar is present. This should include a current test with a long duration to verify whether the edge scour hole is able to undermine the collar and finally reach the pile perimeter and a series of subsequent tests with a storms and current-only conditions to study the effect of varying hydrodynamic loads and the role of initial edge scour.
- Fixation of the collar at a certain height above the seabed may worsen the scour problem under wave-dominated conditions. It should be investigated whether natural seabed variations (e.g. ripples or sand waves) could make the collar counter-effective.
- A sufficiently long skirt can prevent scour at the pile. Therefore, the minimum required skirt length and the fixation of the skirt to the pile should be further investigated.
- The effect of tidal flow was not considered. Tide reversal may have an effect on the timescale of scour development.
- A flexible collar may be more effective than a stiff collar, providing that it is

flexible enough to follow edge scour development, but heavy enough to prevent uplift under wave action. Additional research is required to confirm this.

- In cooperation with the industry, integrated foundation design and installation methods should be evaluated in order to provide insight into the (economical) feasibility of applying collars to monopiles.

Furthermore, an interpretation is needed to translate the results obtained in the model to reality. Options to consider are scaling the number of waves or using a sediment transport based approach.

REFERENCES

Hoffmans, G.J.C.M., Verheij, H.C., (1997). "Scour Manual". Balkema, Rotterdam, The Netherlands.

Kumar, V., Raju, K.G.R and Vittal, N., (1999). "Reduction of Local Scour around Bridge Piers Using Slots and Collars." *Journal of Hydraulic Engineering*. Vol 125. No 12. December 1999

Raaijmakers, T.C., Rudolph, D., (2008). "Time-dependent scour development under combined current and waves conditions - laboratory experiments with online monitoring technique." *Fourth International Conference on Scour and Erosion*, Tokyo 2008.

Rudolph, D., Raaijmakers, T.C., (2007). "Scour around jack-up legs with cone-shaped footings and skirts." *11th International Conference "The Jack-Up Platform Design, Construction & Operation"*, 11-12 September 2007, City University, London, England

Sheppard, D.M., Miller Jr., W., (2006). "Live-Bed Local Pier Scour Experiments". *Journal of Hydraulic Engineering*, Vol. 132, No. 7.

Simon, J.M., Johansen, N., Danyluk, R., (2009). "Design and Experimental Testing of New Scour Prevention Deveices for Offshore Wind Turbine Monopile foundations." *Proceedings of European Offshore Wind Conference*, Stockholm, Sweden, 14-16 September 2009.

Sumer, B.M., Freds¢e, J., (2002). "The mechanics of scour in the marine environment." *Advanced Series on Ocean Engineering* - Volume 17. New Jersey: World Scientific.

Whitehouse, R.J.S. (1998). "Scour at marine structures". London: Thomas Telford Limited.

Three-Dimensional Scour at Submarine Pipelines In Unidirectional Steady Current

Yushi Wu[1] and Yee-Meng Chiew[2], Member, ASCE

[1] Research Engineer, Nanyang Technological University, DHI-NTU Water & Environment Research Centre and Education Hub, School of Civil and Environmental Engineering, Nanyang Avenue, Singapore 639798.
[2] Professor, Nanyang Technological University, School of Civil and Environmental Engineering, Nanyang Avenue, Singapore 639798. Tel.: +65-6790-5256; fax: +65-6791-0676; e-mail: cymchiew@ntu.edu.sg (author for correspondence)

ABSTRACT

This paper presents results of an experimental study on 3-dimensional scour at submarine pipelines with uniform sediments under a unidirectional steady current. A dimensional analysis is first conducted to identify all the important non-dimensional parameters. Laboratory experiments are then conducted to study the development of a 3-dimensional pipeline scour hole under different sets of environmental conditions. The results are recorded and the corresponding propagation velocities of the free span calculated. The effects of four parameters on the propagation velocity are studied through the conduct of several groups of experiments; each of which exclusively focuses on one particular parameter. Moreover, the scour pattern under different combinations of environmental conditions is discussed to obtain an improved understanding on the mechanism of scour hole propagation at the span shoulder of pipelines.

INTRODUCTION

Since scouring has been recognized as one of the major causes of submarine pipeline failure, numerous studies have been conducted in this area over the past 30 years. Although pipeline-scour holes are actually 3-dimensional in the field, most published experimental studies and numerical modelling of pipeline-scour are performed with a 2-dimensional model (Sumer and Fredsøe, 2002). This is because of the expense associated with building physical models in the laboratory and high demand on computational capacity related to numerical simulations. To better understand the development of a scour hole at submarine pipelines in the field, this study aims to examine the 3-dimensional characteristics of pipeline-scour.

The development of 3-dimensional scour includes the following behaviors: (1) lateral propagation of the scour hole; (2) free span behavior: vibrating and sagging; (3) pipeline sinking at the span shoulders due to shear failure; and (4) self-burial of, or deposition at the pipeline. The objective of the present study focuses on the first process, i.e., propagation of the 3-dimensional scour hole at pipelines, which is characterized by the scour hole dimensions at different time stages and the propagation velocity of the scour hole along the pipeline axis (Fig.1), V_L, which is defined by:

$$V_L = \frac{dL}{dt} \tag{1}$$

in which L = length of the scour hole as shown in Fig. 1; and t = time.

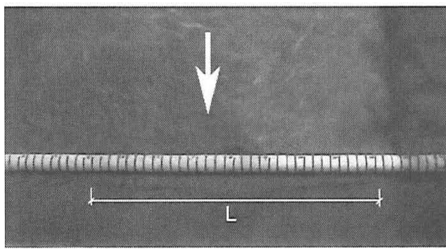

Figure 1 Top view of a scour hole

DIMENSIONAL ANALYSIS

A dimensional analysis is performed to identify the dimensionless parameters, which are likely to influence the propagation velocity of the scour hole. The dependant variable that the present study focuses on is V_L. The variables that affect V_L include: mean flow velocity of the approach flow, V (on the assumption of a fully developed boundary layer); undisturbed approach flow depth, y_n; density of water, ρ; density of the sediment, ρ_s; viscosity of water, μ; channel width, B; median grain size of bed material, d_{50}; diameter of the pipeline, D; pipeline embedment, e, where e = vertical distance between the bottom of the pipeline to the undisturbed sediment bed level (In this study, a positive value of e means that the pipeline is buried in the sediment bed); and acceleration due to gravity g (Moncada-M and Aguirre-Pe, 1999). Dey and Singh (2008) have reported other variables, which also could influence the pipeline scouring such as geometric standard deviation of the bed sediment, σ_g and shape of the pipeline cross section. In this study, σ_g, however, is a dimensionless constant and the shape of all pipeline models tested is circular. Consequently, σ_g and the shape of the pipeline cross section are not considered in the following dimensional analysis. Some of the variables discussed above are schematically defined in Fig. 2.

As a result, the scour process is expressed functionally as:

$$V_L = f(V, y_n, \rho, \rho_s, \mu, B, D, d_{50}, e, g) \tag{2}$$

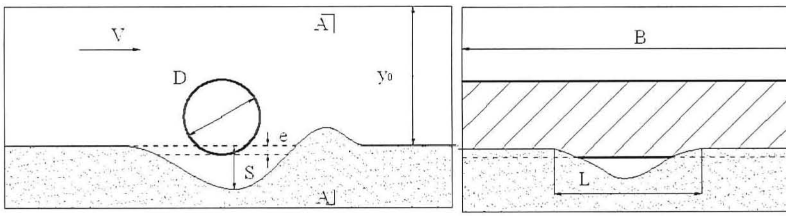

(a) (b)

Figure 2 Schematic definition of variables.
(a) Side view of the test section; (b) front view of the test section along A-A

According to Buckingham's Pi theorem, with the selection of V, D, ρ as the basic repeating variables, eight independent non-dimensional parameters are obtained as follows:

$$\Pi_1 = \frac{V_L}{V} \tag{3}$$

$$\Pi_2 = \frac{B}{D} \tag{4}$$

$$\Pi_3 = \frac{e}{D} \tag{5}$$

$$\Pi_4 = \frac{y_n}{D} \tag{6}$$

$$\Pi_5 = d_* = d_{50}\left[\frac{g(s-1)}{\nu^2}\right]^{1/3} \tag{7}$$

$$\Pi_6 = \mathrm{Re} = \frac{VD\rho}{\mu} \tag{8}$$

$$\Pi_7 = \mathrm{F} = \frac{V}{\sqrt{gy_n}} \tag{9}$$

$$\Pi_8 = \theta = \frac{U_*^2}{g(s-1)d_{50}} \tag{10}$$

in which $\frac{V_L}{V}$ = dimensionless propagation velocity; $\frac{B}{D}$ = flume width to pipeline diameter ratio; $s = \frac{\rho_s}{\rho}$, specific gravity of sediment grains; d_* = dimensionless particle parameter; Re = Reynolds Number; F= Froude Number; $\frac{e}{D}$ = embedment to pipeline diameter ratio; $\frac{y_n}{D}$ = water depth to pipeline diameter ratio, and θ = Shields parameter, in which U_* = undisturbed friction velocity, which can be calculated using the mean velocity equation for a rough bed as follows:

$$\frac{V}{U_*} = 5.75 \log \frac{y_n}{2d_{50}} + 6 \qquad (11)$$

It is noted that d_* does not vary in all the experiments in this study because only one type of sediment is used; the influence of $\frac{B}{D}$ is assumed negligible because the flume is relatively wide with $\frac{B}{D} \geq 13.8$; Reynolds Number effects are also excluded because it had been demonstrated to have a weak influence on the scour process by Moncada-M and Aguirre-Pe (1999) and Sumer and Fredsøe (2002) for a smooth pipeline in the range of Reynolds number ($4.00 \times 10^3 \leq \text{Re} \leq 2.16 \times 10^4$) used in the current study. The remaining four parameters $\frac{e}{D}, \frac{y_n}{D}, \theta$ and F are tested systematically in the study.

EXPERIMENT SET-UP

All the experiments are conducted in a glass-sided flume that is 19.0 m long, 1.6 m wide and 0.45 m deep at the Hydraulic Modeling Laboratory, Nanyang Technological University, Singapore. A 1.5 m long sediment recess with depth = 150 mm is located 14.0 m downstream from the flume inlet. Fig. 3 shows how seven Perspex plates with the same sand as that in the test section glued on top are fixed to the bottom of the flume as the false floor. Five of them are located upstream and two downstream of the test section. Two sets of dowel pegs with height = 100 mm are installed at the location 4.0 m downstream from the flume inlet. The purpose of the dowel pegs and roughened false floor is to assist the formation of a fully developed boundary layer. Before the actual scour experiments are conducted, the center-line flow velocity profile at the location where the pipeline is installed is measured and confirmed to conform to Eq. (11).

Uniform sand with median grain size d_{50} = 0.56 mm and geometric standard deviation σ_g = 1.4 is used in the study. Eight model PVC cylinders with diameters = 22 mm, 26 mm, 32 mm, 35 mm, 38 mm, 49 mm, 60 mm and 116 mm are used as modeled pipelines.

All the experiments are arranged in four groups, with each group focusing on the study of the effect of one of the four parameters derived earlier. Consequently, only one parameter is changed in each group between individual tests while all the others are kept constant. Experiments Series A, B, C and D focus on studying the effect of pipeline embedment ratio, e/D ($0.00 \le e/D \le 0.30$), water depth to pipeline diameter ratio, y_n/D ($1.72 \le y_n/D \le 7.69$), Shields parameter, θ ($0.009 \le \theta \le 0.021$ or $0.549 \le U_*/U_{*cr} \le 0.828$. U_{*cr} = critical friction velocity corresponding to the initiation of motion of the bed sediment) and Froude number, F ($0.155 \le F \le 0.249$), respectively.

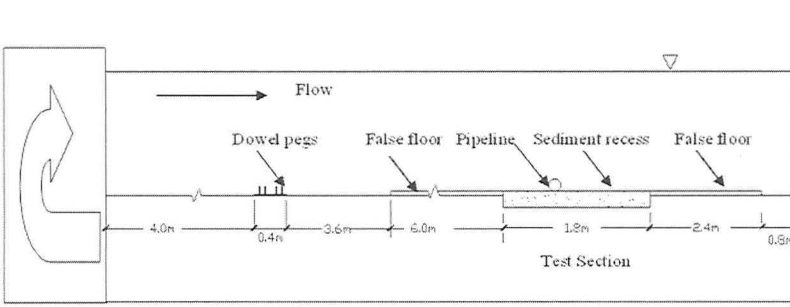

Figure 3 Side view of the flume and set up

RESULTS AND DISCUSSION

The following section discusses the development of 3-dimensional pipeline scour in steady current based on the observation and data of propagation velocity calculated from the experiments. Besides, this paper reports the effect of Shields' parameter, θ and Froude number, F on V_L/V. In this study, the propagation velocity, V_L is determined by computing the gradient of the temporal development curve of the free span length of a 3-dimensional scour hole.

Temporal Development of 3-Dimensional Scour hole

With different combinations of environmental conditions and pipeline embedment ratios, the temporal development of a 3-dimensinoal scour can be significantly different, both in terms of the propagation velocity and development pattern. Fig. 4 shows the temporal development of the free span length with different e/D ($0.00 \le e/D \le 0.30$). The pipeline model is rigid and fixed to the flume walls so that it cannot sag or sink when the scour is developing, which means that e = constant in each experiment. The scour propagation velocity, which can be calculated from the gradient of the curves, clearly decreases with increasing e/D.

A closer examination of the measured data reveals that the development of the free span can be divided into two stages, namely a rapid and slack phase of development. In the former phase, the scour hole propagates with a higher, but relatively constant rate. In the light of this, the temporal development curve of the free span length at this stage of development is a steep, straight line. With the latter phase, V_L is conspicuously smaller and continues to decrease gradually as the scour hole develops.

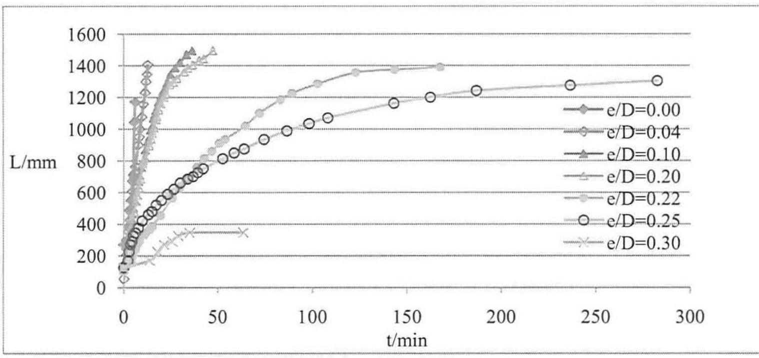

Figure 4 Temporal development of free span with different e/D for y_n/D=4.08, F=0.171 and θ= 0.018

The data also show that as e/D increases, the rapid phase of development becomes less prominent. Its occurrence is confined to a shorter duration with a smaller gradient, dL/dt, and hence, V_L. When the rapid phase of development diminishes with time, the slack phase of development begins to take over and dominate the scouring process. The interface between these 2 phases of development is represented by a sudden change of the gradient as shown in Fig. 4. As e/D increases beyond approximately 0.2, no clear rapid phase can be detected from the temporal development curve of the free span length, and the slack phase completely dominates the scour hole development. In summary, the patterns of 3-dimensional pipeline scour propagation can be reduced to three situations: rapid-phase dominant, rapid and slack phase co-existent and slack-phase dominant.

In the rapid-phase dominant situation, observation shows a violent ejection of sediment particles from beneath the pipeline at the span shoulders. This injection is due to a strong local seepage flow in the sand below the pipeline, sometime even causing piping. A few of the temporal development curves under this situation are able to reach a length in excess of 87% of the overall width of the flume. This occurs when piping is present beneath the pipe with a relatively small embedment ratio. Under the rapid and slack phase co-existent condition, the rapid phase is less prominent with no apparent ejection of sediment particles or piping. The slack phase of development is short but reduction of the propagation velocity is very obvious. The development turns to slack-phase dominant when $e/D > 0.2$, in which the rapid phase only occurs at the very beginning stage of the scour hole development and ceases altogether later. The slack-phase dominant condition is characterized by an extremely slow development of the free span length, sometimes stopping totally after a short duration after the beginning of scour. For example, for $e/D = 0.30$, scouring or elongation of the scour hole ceases 35 minutes after the initiation of scouring. After this, backfilling takes over and the pipeline is partially buried, similar to those observed by Chiew (1990) in 2-dimensional pipeline-scour tests.

Figures 4, 5 and 6 present the temporal development of the scour hole with varying e/D, y_n/D and V/U_{cr}, respectively. A cursory comparison of these 3 sets of experiments reveals that the temporal development patterns are very similar. It proves the universality of the two phases of development associated with 3-dimensional scour at pipelines. Furthermore, a variation of each of these parameters may result in similar changes to the temporal development of 3-dimensional scour. Some parameters, e.g. V/U_{cr}, represent the environment force. Hence, the increase of each of these parameters will tend to enhance the scour process. The others, e.g. e/D, y_n/D, represent the stability force; an increase of which will tend to render the pipeline more stable and inhibit scour. In view of this, the evolution of the development patterns of a 3-dimensional sour hole is determined by the balance between the environment force and the stability force. Since the intensity and speed of the scour process is very different in the two phases of development, studies to quantify these two forces and the criterion to predict the 3-dimensional scour pattern under pipelines have great engineering significance.

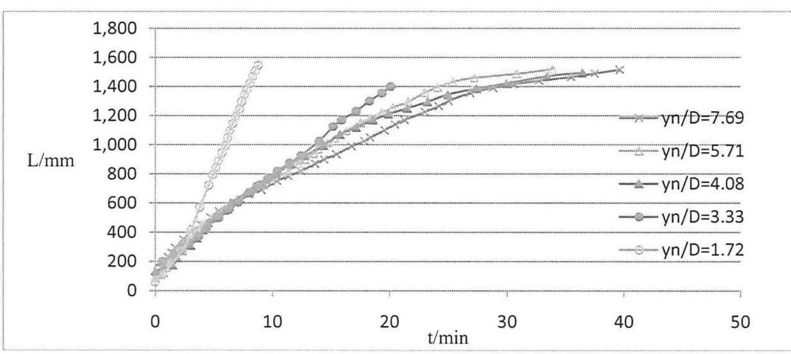

Figure 5 Temporal development of free span with different y_n/D for e/D=0.1, F=0.171 and θ= 0.018

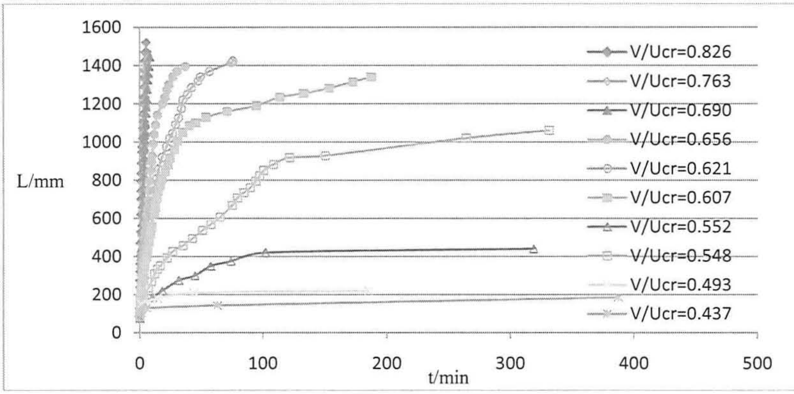

Figure 6 Temporal development of free span with different V/U_{cr} for e/D=0.1 and y_n/D=4.08

Effect of Froude number, F and Shields parameter, θ

When the average flow velocity, V is changed, the Froude number, F and Shields parameter, θ are changed because they are both functions of V and thus not independent to each other. In order to examine the effect of one parameter without contribution from the other, F is changed while θ is kept constant and vice versa. The results are shown in Figs. 7 and 8.

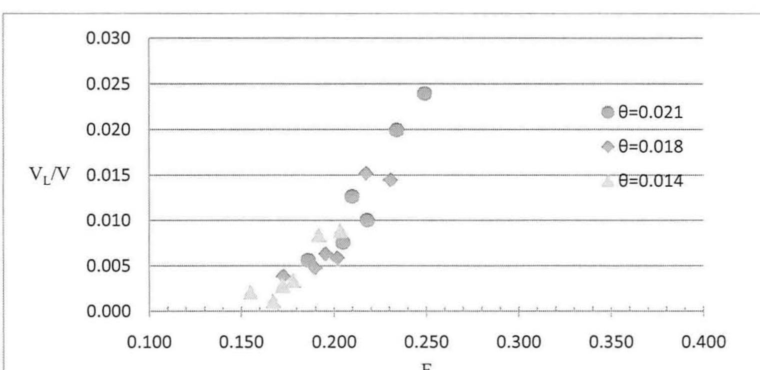

Figure 7 Non-dimensional propagation velocity versus Froude number, F for e/D=0.1 and y_n/D=4.08

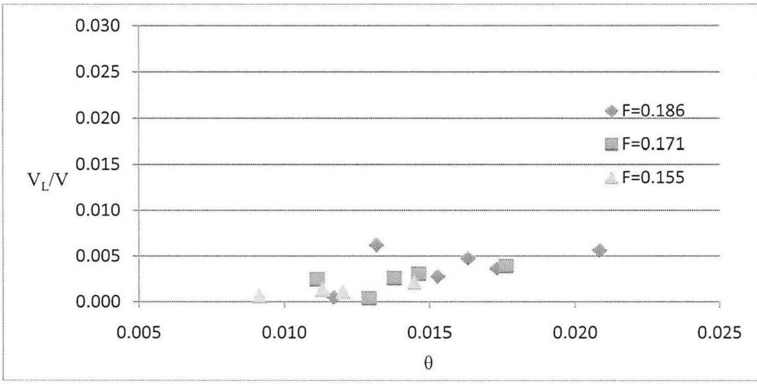

Figure 8 Non-dimensional propagation velocity versus Shields parameter, θ for e/D=0.1 and y_n/D=4.08

Fig. 7 shows that the non-dimensional propagation velocity, V_L/V increases dramatically with increasing F ($0.141 \leq \mathrm{F} \leq 0.249$) for e/D= 0.1 and y_n/D= 4.08. The dependent relationship of V_L/V on F is very clear. The fact that all the data with different θ values collapse into one graph implies that V_L/V is mainly dependent on F while θ has comparatively little effect in the range of $0.014 \leq \theta \leq 0.021$ ($0.549 \leq U_*/U_{*cr} \leq 0.828$). The variation of V_L/V on θ in Fig. 8 confirms the inference above. The data in Fig. 8 hardly show any significant change of V_L/V with varying θ in the above mentioned range.

Figures 9 (a), (b) and (c) show the comparison of the variation of V_L/V on V/U_{cr}, θ and F with the same data, respectively. Since the three parameters which are all able to represent the magnitude of the incoming flow velocity, V, the data are grouped with different pipeline diameters. In this way, the only variable in each group is V, while all the other variables remain constant. The curves of V_L/V with different pipeline models collapse into one when they are plotted against F as shown in Fig. 9 (c), which proves that F is the controlling parameter that determines the value of V_L/V and the other two are insignificant when all the other parameters are kept constant. Based on their experiments, Cheng et al. (2009) concluded that V_L/V increases as θ increases. In their study, when θ changes, F also changes. In other words, the trend of V_L/V in Cheng et al.'s (2009) result is not only under the influence of θ, but also F. In this way, the actual parameter changed is V/U_{cr}, while θ only acts as a representative of V/U_{cr}.

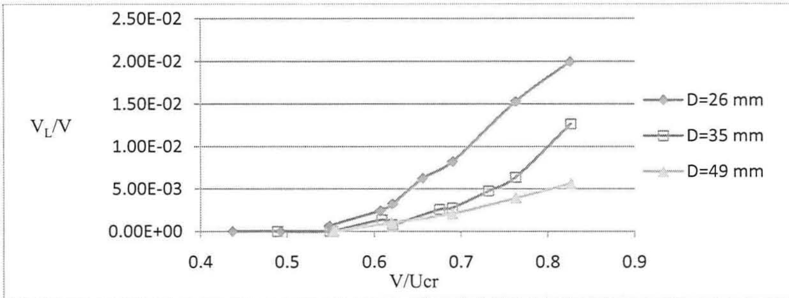

(a)

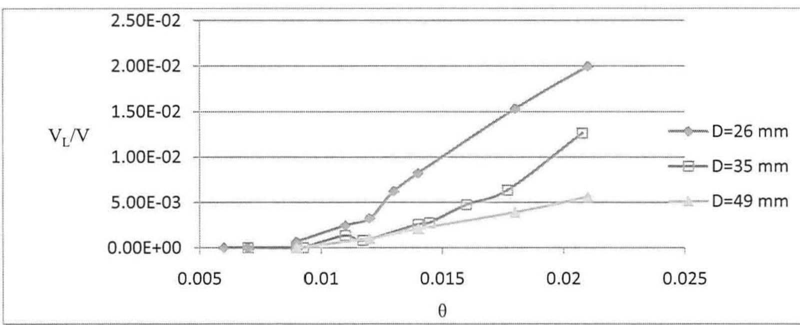

(b)

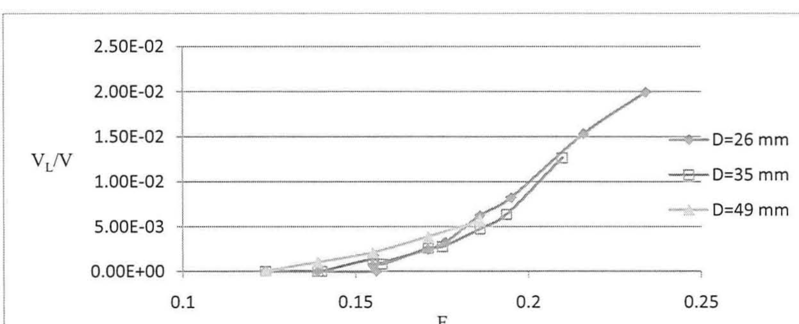

(c)

Fig. 9 Comparison of the dependence of V_L/V on (a) V/U_{cr}, (b) F and (c) θ

In summary, the present study shows that Froude number F for $0.155 \leq F \leq 0.249$ is a very influential parameter in affecting V_L / V of the 3-dimensional scour hole, while Shield parameter θ for $0.009 \leq \theta \leq 0.021$ ($0.549 \leq U_* / U_{*cr} \leq 0.828$) hardly has any effect on V_L / V .

CONCLUSIONS

The following conclusions can be drawn based on the results presented in this study:

1. The development of the 3-dimensional pipeline scour can be divided into a rapid phase and slack phase. In the rapid phase of development, the scour hole propagates in a faster and constant velocity; while in the slack phase of development, the scour hole propagates in a slower and reducing velocity.

2. The temporal development of the 3-dimensional pipeline scour exhibits three patterns, namely, (1) rapid-phase dominant, (2) rapid and slack phase co-existent and (3) slack-phase dominant, which is determined by the balance between environmental force and stability force.

3. The propagation velocity is very sensitive to Froude number, F for $0.155 \leq F \leq 0.249$, but not so to Shields parameter, θ in the range of current study $0.014 \leq \theta \leq 0.021$ ($0.549 \leq U_* / U_{*cr} \leq 0.828$).

ACKNOWLEGEMENT

The authors acknowledge the support from DHI-NTU Water & Environment Research Center and Education Hub.

REFERENCES

Cheng, L., Yeow, K., Zhang, Z., Teng, B. (2009). "Three-dimensional scour below offshore pipelines in steady currents". *Coastal Engrg. J.* 56: 577-590.

Chiew, Y.M. (1990). "Mechanics of Local Scour Around Submarine Pipelines". *J. Hydraulic Engrg.*, ASCE. 116: 515-529.

Dey, S., Singh, N.P. (2008). "Clear-water scour depth below underwater pipelines". *J. Hydro-environment Research.* 1 (2): 157-162.

Moncada-M, A.T., Aguirre-Pe, J. (1999). "Scour below pipeline in river crossings". *J. Hydraulic Engrg.*, ASCE. 125: 953-958.

Sumer, M. B., Fredsøe, J. (2002). "The Mechanics of Scour in the Marine Environment". World Scientific, Singapore.

Numerical Model for Three-Dimensional Scour Below a Pipeline in Steady Currents

Liang Cheng[1] and Ming Zhao[2]

[1]School of Civil and Resource Engineering, The University of Western Australia, 35 Stirling Highway, Crawley, WA 6009, Australia, PH +61 8 6488 3076; email: cheng@civil.uwa.edu.au
[2]School of Civil and Resource Engineering, The University of Western Australia, 35 Stirling Highway, Crawley, WA 6009, Australia, PH +61 8 6488 7356; email: zhao@civil.uwa.edu.au

ABSTRACT

A three-dimensional numerical model is established for simulating scour propagation in spanwise direction under a sub-sea pipeline in steady currents. In the model, flow is simulated by solving the Reynolds averaged Navier-Stokes equations with a k-ω turbulence model. The bed development is modelled by conservation of sediment mass. Calculations are carried to simulate local scour development below a pipeline that has been investigated experimentally. The input conditions of the simulation are set as closely as possible to those used in the physical tests reported in literature. The embedment depth of the pipeline was 0.2 pipeline diameter. It was found that scour development in the spanwise direction is mainly caused by the flow velocity around the span shoulders, where the gap between pipeline and bed is small. In the middle of the scour hole, the scour process is similar to that observed in the 2D laboratory tests and 2D numerical results reported in previous studies. The simulation demonstrates the capability of the 3D model although the calculated propagation speed of scour hole in the spanwise direction of pipeline is slightly lower than that measured in the tests.

INTRODUCTION

When a sub-sea pipeline is laid on an erodible sea-bed, local scour below the pipeline will happen under certain flow conditions. Local scour may be unfavourable to pipeline stability because it increases hydrodynamic forces and leads to vortex-induced vibrations of the pipeline.

Local scour around a sub-sea pipeline has been investigated intensively both experimentally and numerically in the past decades due to its significance in offshore engineering (Brørs, 1999; Mao, 1986; Lu et al., 2005; Sumer et al., 1988; Li and Cheng 1999 and 2001; Zang et al., 2009; Zhao and Cheng, 2008). Most studies conducted so far, either by experimental methods or by numerical methods, were two-dimensional (2D). Mechanisms of 2D scour below a pipeline such as piping, tunnel scour and lee wake scour are well understood. Scour below a pipeline in real life always takes place in three dimensional fashion. Onset of scour will initially happen at one section below the pipeline and the scour will extends in both transverse and the spanwise directions with respect to the pipeline. Two dimensional scour models can predict well the scour process in the transverse plane of the pipeline. However, the scour development in the spanwise direction of the pipeline has been beyond the capacity of 2D models. Studies on three-dimensional scour below pipelines are rare. Bernetti et al. (1990) proposed a theoretical model for analysing the longitudinal propagation of a scour hole based on the sediment conservation equation. It was assumed that the slope of the scour hole at span shoulders is equal to the natural angle of repose of the sediment bed. This model was later adapted by Hansen et al. (1991) to account for parameters that may slow down the scouring process such as pipeline embedment and sagging. The lowering of the pipeline, due to increased span length, was found to significantly increase the time taken for the free span to develop. Furthermore the embedment depth was found to influence free span developments. Recently Cheng et al. (2009) studied three-dimensional scour below a pipeline under steady currents by a series of laboratory tests and they developed empirical formulae for predicting speed of propagation of scour in the spanwise direction.

In this study, a three-dimensional numerical model is established for simulating scour below a sub-sea pipeline. The flow is simulated by the finite element model developed by Zhao et al. (2009). Both bed load and suspended load are considered in the sediment transport. Bed load is calculated by empirical formula and suspended load is solved by the convection-diffusion equation of sediment concentration in water. The bed evolution is predicted by solving the conservation equation of sediment mass. The sediment concentration equation and the bed evolution equation are also solved by finite element method. Calculations were carried out under the same conditions as those measured in the tests by Cheng et al. (2009). The embedment depth of the pipeline was 0.2 pipeline diameter. It was found that scour development in the spanwise direction is mainly due to large flow velocity around the span shoulders, where the gap between pipeline and bed is small. In the middle section of the free span, the scour process is similar to that observed in the 2D laboratory tests and 2D numerical results in previous studies. The simulation results demonstrate the capability of the 3D model, although the calculated propagation speed of scour hole in the spanwise direction of the pipeline is lower than that measured in the tests.

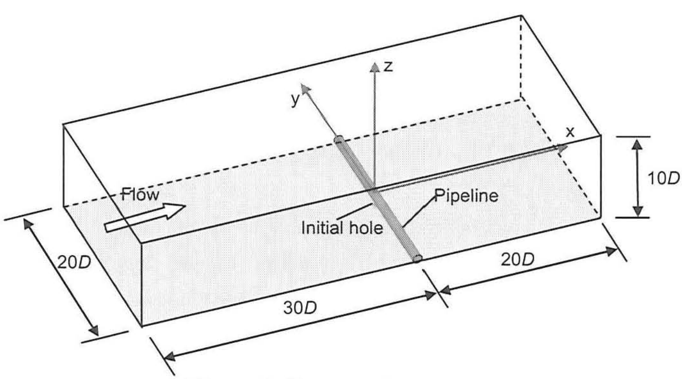

Figure 1. Computational domain

NUMERICAL METHOD

Figure 1 shows the computational domain for the flow and scour simulation. D is the pipeline diameter in Figure 1. The turbulent flow around a sub-sea pipeline is simulated by solving the Reynold-Averaged Navier-Stokes (RANS) equations and k-ω turbulence equations. The RANS in a computational domain with a continuously changing bed boundary are solved by Arbitrary Lagrangian Eulerian (ALE) scheme. In ALE scheme the position of each mesh node moves and convection terms are modified in order to consider the effects of the mesh moving speed. The RANS are expressed as

$$\frac{\partial u_i}{\partial t}+\left(u_j-u_{jp}\right)\frac{\partial u_i}{\partial x_j}=-\frac{1}{\rho}\frac{\partial p}{\partial x_i}+\frac{\partial}{\partial x_j}\left[\nu\frac{\partial u_i}{\partial x_j}+\tau_{ij}\right] \tag{1}$$

$$\frac{\partial u_i}{\partial x_i}=0 \tag{2}$$

where x_i (i = 1, 2 and 3) is the Cartesian coordinates, u_i is the velocity component in x_i direction, p is the pressure, ν is the kinematic viscosity, t is time, ρ is the fluid density, u_{jp} is the velocity of the computational mesh movement, τ_{ij} is the Reynolds stress which is defined as $\tau_{ij}=\nu_t\left(\partial u_i/\partial x_j+\partial u_j/\partial x_i\right)-(2/3)k\delta_{ij}$, k is the turbulent energy, ν_t is the turbulence viscosity. The k-ω SST (shear-stress transport) model (Menter, 1994) is employed to solve the turbulence. Menter (1994) reported that this turbulence model gave better results in flows where strong adverse pressure gradients exist.

The governing equations were solved using the finite element model (FEM) developed by Zhao et al. (2009). In this model a Petrov-Galerkin finite element scheme was employed in three-dimensional flow simulation. Detail of the FEM model used in this study can be found in Zhao et al. (2009).

Bed load and suspended load are considered in the numerical model. A reference level z_a is specified, below which the sediment movement is considered to be in the form of bed load and above which the sediment transport is considered to be suspended load. The z_a in the present paper is set to be $2d_{50}$, with d_{50} being the median sediment grain diameter. The suspended sediment was evaluated by volume concentration (c), which was computed by solving the convection-diffusion equation

$$\frac{\partial c}{\partial t}+\left(u_j-u_{jp}\right)\frac{\partial c}{\partial x_j}-w_s\frac{\partial c}{\partial x_3}=\frac{\partial}{\partial x_j}\left(\sigma_c\nu_t\frac{\partial c}{\partial x_j}\right) \tag{3}$$

where σ_c is a constant which is set to be 1 in this paper, w_s is the fall velocity of the sediment particles in still water. Eq. (3) is solved by same method used by Zhao et al. (2010). The reference concentration (c_a) at the reference level ($2d_{50}$ above bed) is calculated using the empirical formula proposed by Zyserman and Fredsøe (1990)

$$c_a=\begin{cases}0.331(\theta_s-0.045)^{1.75}/\left(1+0.72(\theta_s-0.045)^{1.75}\right), & if\ \theta_s>0.045\\ 0, & if\ \ \theta_s\le 0.045\end{cases} \tag{4}$$

The skin friction Shields parameter θ_s is calculated by $\theta_s=u_{fs}^2/[g(s-1)d_{50}]$ and the skin friction velocity u_{fs} is obtained according to the logarithmic law by $u_{fs}=\kappa u_T/\ln(\Delta_1/z_{0s})$, where u_T is the velocity at the mesh node next to the wall, Δ_1 is the distance between the wall and the mesh node. Bed load transport rate $\mathbf{q}_b=(q_{bx},q_{by})$ is calculated by the semi-empirical equation proposed by Engelund and Fredsøe (1976)

$$\mathbf{q}_b=\frac{\pi d_{50}^3}{6}\frac{P_{EF}}{d_{50}^2}\mathbf{U}_b \tag{5}$$

where $\mathbf{U}_b$ is the velocity of the sediment movement, P_{EF} is the percentage of the particles that are moving on the bed, which is calculated by

$$P_{EF} = \left[1 + \left(\frac{\pi\mu_d/6}{\theta - \theta_c}\right)^4\right]^{-1/4} \tag{6}$$

When sediments move along a sloped bed as shown in Fig. 11, the critical Shields parameter is modified as (Zhao and Teng, 2001; Roulund et al., 2005)

$$\theta_c = \theta_{c0}\left[\sqrt{\cos^2\beta - \frac{\sin^2\beta\sin^2\alpha}{u_s^2}} - \frac{\cos\alpha\cos\beta}{\mu_s}\right] \tag{7}$$

in which θ_{c0} is the critical Shields parameter for a flat bed, $\mu_s = \tan\phi_s$ is the static friction coefficient, β is the bed slope angle, α is the angle between the down-slope direction and the bed shear stress. The sediment movement speed $\mathbf{U}_b$ in Eq. (5) is calculated according to the force equilibrium of the moving particles (Roulund et al. 2005). Details about calculating $\mathbf{U}_b$ can be found in Roulund et al. (2005).

Bed evolution is modelled by solving the mass balance equation of the sediment (Brørs, 1999; Liu and Garcia, 2008; Zhao et al., 2010)

$$\frac{\partial z_b}{\partial t} = \frac{1}{1-n}\left[-\nabla \cdot \mathrm{q}_b + D_s - E_s\right] \tag{8}$$

where D_s is the deposition rate defined as $D_s = w_s c_b$, the erosion rate $E_s = w_s c_a$, c_b is the sediment concentration at the reference level. In the fully developed straight channel flow where the erosion and deposition are balanced at the reference level i.e. $c_b = c_a$. In order to save computational time, the morphological time step is set larger than the flow time step (Brørs, 1999; Liang, et al., 2005; Zhao and Cheng, 2008). The method for choosing morphological time step Δt_b is the same as the one used by Zhao and Cheng (2008). The criteria for choosing Δt_b are: (1) bed change within one morphological time step is less than 0.0005 times of pipeline diameter (D) and (2) $\Delta t_b \le 10\Delta t$ with Δt being the flow time step. Both criteria have to be satisfied. According to the criteria, the morphological time step is less than $10\Delta t$ in the early stage of scour and equal to $10\Delta t$ at the later stage of scour. Parallel computational code is developed and all the computations in this study are carried out on the WASP (Western Australian Supercomputer Program). The WASP has 164 dual core 2.6 GHZ AMD opteron processors, with a total of 328 (164×2) cores. A total of 64 cores on the cluster were used for the simulation.

NUMERICAL RESULTS

Numerical simulations are carried out to simulate 3D scour below a pipe in a laboratory scale for the purpose of comparing numerical results with experimental data. The tests conducted by Cheng et al. (2009) are selected for this purpose. Cheng et al. (2009) carried laboratory tests about 3D scour around sub-sea pipelines in a water flume of 2.5 m in height, 4 m in width and 50 m in width. The simulations are carried out under the same conditions as test case of C450e2 by Cheng et al. (2009). The calculation parameters are: model pipeline diameter is 0.05 m, water depth is 0.5 m, flow velocity (measured at one pipeline diameter above bed) is U=0.33 m/s, median sediment size is d_{50}=0.4 mm. In the numerical simulation, the pipeline length is 1 m (20*D*), which is smaller than that used in the test (4m). It is expected the scour process will not be affected by the pipeline length before the scour reaches the two ends of the pipeline. Figure 2 (a) shows the 3D computational mesh after scour has developed below the pipeline. The 3D computational mesh comprises layers of 2D meshes with a constant interval in the pipeline's spanwise direction. Eight-node hexahedron elements are used to discretize the computational domain. Figure 2 (b) shows the mesh at the centre of the pipeline where significant scour has developed. Figure 2 (c) shows the mesh at the end of the pipeline where scour has not happened beneath the pipeline. In Figure 2 (c), there are no mesh elements below the pipeline. FEM elements are allocated below the pipeline only when the scour arrives at the location and a gap between pipeline and sea-bed is initiated.

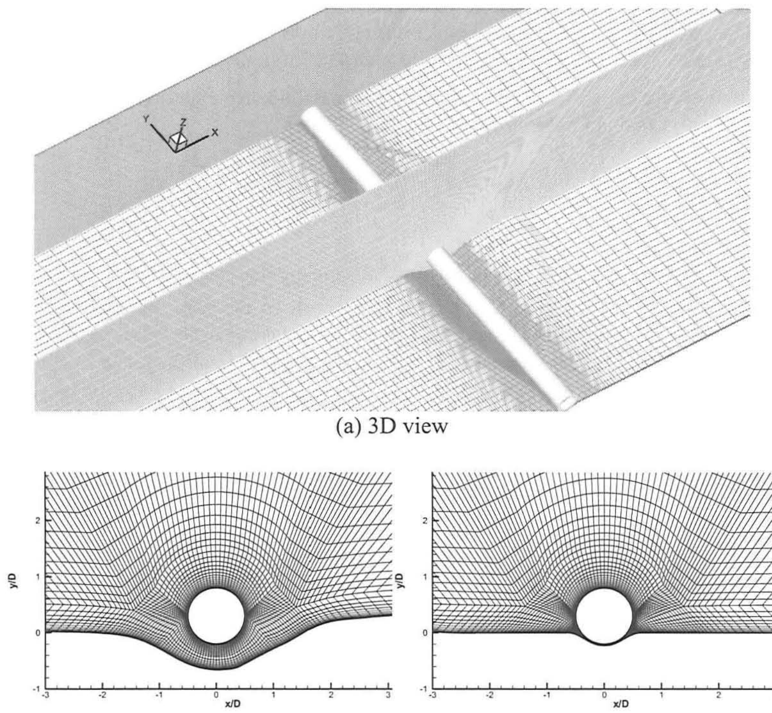

(a) 3D view

(b) xz-plane at centre of the pipeline

(c) xz-plane at end of the pipeline

Figure 2. Computational mesh (coordinate system is defined in Figure 1)

Figure 3 shows three-dimensional scour development according to numerical results. Scour mechanisms observed in the laboratory test were well predicted by the numerical method. At t=170 s, the sediment under the pipeline centre has been washed downstream and piled up right behind the pipeline. The sand dune behind the pipeline grows in its hight and width as more sands are washed to downstream. The propagation of scour can be clearly observed in Figure 3. At t=505 s, scour propagates to the ends of the pipeline. Around the two span shoulders, where the pipeline is supported by the soil, the flow is fully three-dimensional and streamline contraction was observed from the numerical results.

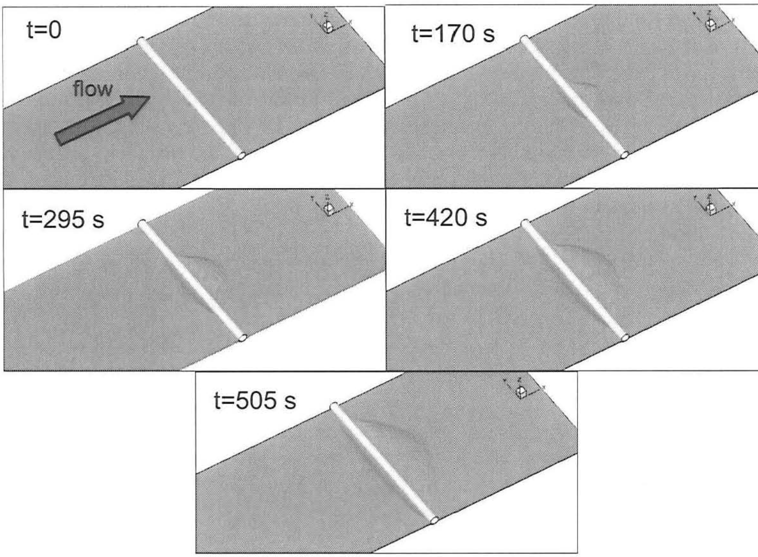

Figure 3. Numerical results of three-dimensional scour development

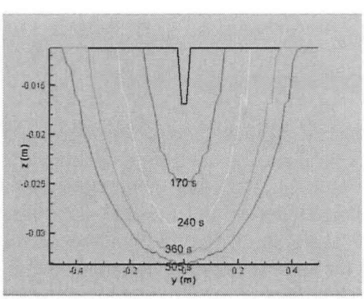

(a) Bed profile in yz-plane

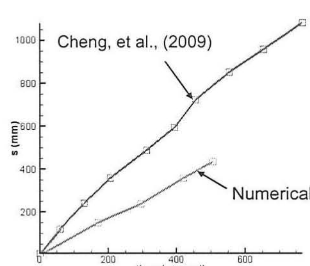

(b) Development of width of scour hole in spanwise direction

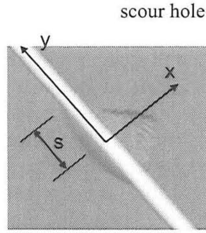

(c) Coordinate-system

Figure 4. development of scour in spanwise direction

Figure 4 (a) shows the development of bed profile in yz-plane. The profiles are symmetric with respect to the y=0 line. The propagation speed of scour in the pipeline's spanwise direction is determined according to the bed profiles in the yz-plane as shown in Figure 4 (a). Figure 4 (b) shows the development of width of scour hole in spanwise direction (S) together with the experimental results by Cheng et al. (2009). The scour propagates to the two ends at almost a constant speed, both in numerical and experimental results. However, the predicted propagation speed is 50% smaller than the experimental results. The reason for the underestimation is not clear. Causes can be attributed to the underestimation such as the effect of the thickness of the boundary layer of incoming flow, the FEM mesh size, the turbulent intensity of incoming flow, the constant parameters used in the sediment transport model, etc. More work is still needed to improve the model.

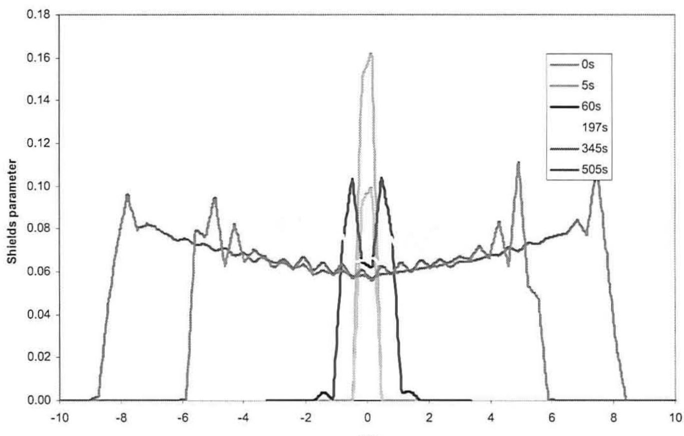

Figure 5. Distribution of Shields parameter along y-axis

Figure 5 shows the distribution of sea-bed Shields parameter along y-axis (spanwise direction). At t=0, sea-bed Shields parameter is very high because of the high velocity jet flow through the initial scour hole. With the development of the scour hole, the Shields parameter at the centre decreases and the non-zero Shields parameter zone widens. It is interesting to see in Figure 5 that the Shields parameter distribution along x-axis is arc shaped with the lowest value at the center and the highest values at the two ends. At the two shoulders, the high Shields parameters produce high sediment transport rates and lead to large scour rates, which contribute to the scour propagation towards the ends of the pipeline. It is understood that sediment particles of the slope can be more easily moved by flow. From Figure 4 it can be seen that the bed slopes at the two shoulders of the suspension are much steeper than the centre part of the pipeline, which also contribute to the scour around the two shoulders. Figure 6 shows three-dimensional streamline around pipelines. The three-dimensionality of the flow at the two shoulders of the suspension can be seen from the streamline picture. It can be seen that upstream the two suspension shoulders, the streamlines bias towards the end of the pipeline.

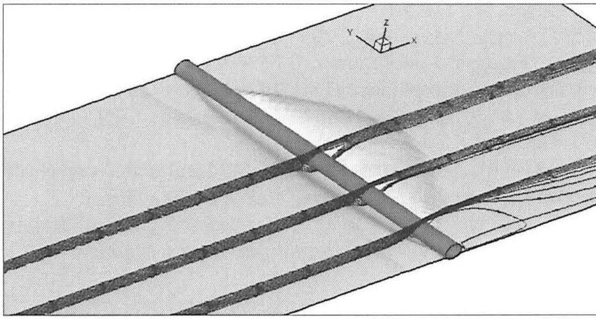

Figure 6. Streamlines around the pipeline

In the study by Cheng et al. (2009), a secondary scour propagation speed is found at the late state of scour. In this study, only primary speed is observed because the pipeline length is not long enough to allow the scour to develop to the secondary state. The development of scour in spanwise direction qualitatively agrees with what was observed in the laboratory test, although the predicted scour propagation speed is smaller than that measured in the test. It should be pointed out that the results shown in this paper are preliminary only. Future work will be focused on improving the accuracy of scour rate prediction and the secondary scour speed.

CONCLUSIONS

A FEM numerical model is established for simulating three-dimensional scour around a sub-sea pipeline. The flow model is based on the Navier-Stokes equations and k-ω turbulent equations. Bed load and suspended load sediment transport rates are considered in the scour model. A preliminary simulation has been carried out under the same conditions as those measured in the laboratory tests by Cheng et al. (2009). By observing the bed profiles at different time instants of scour, the simulated scour process agrees qualitatively with what was observed in the laboratory test. It is found that the high Shields parameter and the steep bed slopes at the two shoulders of the span contribute to the sediment transport and scour propagation in the spanwise direction. The computed scour propagation rate in the spanwise direction is about 50% smaller than the laboratory result. The fundamental mechanism of the scour has been captured by numerical model. Further work will be focused on improving the accuracy of the model.

REFERENCES

Bernetti, R., Bruschi, R., Valentini, V. and Venturi, M. (1990). "Pipelines placed on erodible seabeds." *Proc. 9th International Conference on Offshore Mechanics and Artic Engineering,* ASME, Houston, TX, Vol. V, 155-164.

Brørs, B. (1999). "Numerical modelling of flow and scour at pipelines." *Journal of Hydraulic Engineering* 125 (5), 511 – 522.

Cheng, L., Yeow, K., Zhang, Z., and Teng, B. (2009). "Three-dimensional scour below offshore pipelines in steady currents." Coastal Engineering 56, 577 – 590.

Engelund, F., and Fredsøe, J., (1976). "A sediment transport model for straight alluvial channels." *Nordic Hydrology* 7, 293–306.

Hansen, E.A., Staub, C., Fredsøe, J. and Sumer, B.M. (1991). "Time-development of scour indeuced free spans of pipelines. *Proc. 10th Offshore Mechanics and Artic Engineering Conference*, ASME, Stavanger, Norway, vol. 5, Pipeline Technology, 25-31.

Li, F., and Cheng, L., (1999). "A numerical model for local scour under offshore pipelines." *Journal of Hydraulic Engineering* 125 (4), 400 – 406.

Li, F., and Cheng L., (2001). "Prediction of lee-wake scouring of pipelines in currents." *Journal of waterway, Port, Coastal and Ocean Engineering* 127 (2), 106 – 122.

Liu, X. F., Garcia, M. H., (2008). "Three-dimensional numerical model with free water surface and mesh deformation for local sediment scour." *Journal of Waterway Port Coastal and Ocean Engineering* 134 (4), 203-217

Lu, L., Li, Y. and Qin, J. (2005). "Numerical simulation of the equilibrium profile of local scour around submarine pipelines based on renormalized group turbulence model." *Ocean Engineering* 32 (17-18), 2007 – 2019.

Menter, F. R. (1994). "2-equation eddy-viscosity turbulence models for engineering applications." *AIAA Journal* 32 (8), 1598 – 1605.

Mao, Y. (1986). "The interaction between a pipeline and an erodible bed." *PhD thesis*, Technical University of Denmark, Lyngby, Denmark.

Roulund, A., Sumer, B. M., Fredsøe, J., Michelsen, J. (2005). "Numerical and experimental investigation of flow and scour around a circular pile." *Journal of Fluid Mechanics* 534, 351-401.

Sumer, B. M., Jensen, H. R., and Fredsøe, J., (1988). "Effect of lee-wake on scour below pipelines in current." *Journal of Waterway, Port, Coastal and Ocean Engineering* 114 (5), 599 – 614.

Yeow, K. and Cheng, L., 2004. Local scour around a vertical pile with a caisson foundation, *Proceeding of the 2nd International Conference of Asian and Pacific Coasts* 2003, Paper APAC057 (CD Rom).

Zang, Z., Cheng, L., Zhao, M., Liang, D., and Teng, B. (2009). "A numerical model for onset of scour below offshore pipelines." *Coastal Engineering* 56, 458 – 466.

Zyserman, J. A., and Fredsøe, J. (1990). "Data analysis of bed concentration of suspended sediment." *Journal of Hydraulic Engineering* 129 (9), 1021-1042.

Zhao, M., and Cheng, L. (2008). "Numerical modelling of local scour below a piggyback pipeline in currents." *Journal of Hydraulic Engineering* 134 (10), 1452 – 1463.

Zhao, M., Cheng, L., and Zhou, T. (2009). "Direct numerical simulation of three-dimensional flow past a yawed circular cylinder of infinite length." *Journal of Fluids and Structures* 25, 831 – 847.

Zhao , M., Cheng, L., and Zang, Z. (2010) Experimental and numerical investigation of local scour around a submerged vertical circular. *Coastal Engineering* (*accepted*).

Zhao, M., Teng, B., 2001. Numerical simulation of local scour around a large circular cylinder under wave action. *China Ocean Engineering* 15 (3), 371-382.

Scour Monitoring and Scour Protection Solution for Offshore Gravity Based Foundations

A. Bolle[1], P. Mercelis[1], W. Goossens[1] and P. Haerens[1]

[1] International Marine and Dredging Consultants (IMDC nv), Coveliersstraat 15, 2600 Berchem, Belgium; PH: +32 (0)3 270 92 90; email: annelies.bolle@imdc.be

ABSTRACT

In the first phase of C-Power's offshore wind farm project, six gravity based foundations (GBFs) have been installed 30km offshore of the Belgian Coast, on the Thornton bank in the North Sea. To guarantee the stability of the GBFs, a static scour protection system is designed. One of the challenges during construction is to define a realistic method so that the minimum required layers thicknesses are guaranteed, without placing excessive amounts of material. The feasibility of certain solutions, in relation to the applied equipment and the accuracy of measurements, all have to be taken into account. As a result of numerous discussions between client and contractor, the design has been optimised, been agreed on and immediately tested in practice, during construction of the first phase. Combined with an extensive monitoring program, this allows evaluation of the applied methods.

THE WIND FARM

Location & Construction

C-Power obtained a concession to build and operate a 300MW offshore wind farm for sixty 5MW wind turbines in the Exclusive Economical Zone of Belgium Continental Shelf. The concession area is located on the western part of the Thornton Bank, a sand bank situated approximately 30 km off the Belgian Coast (see Figure 1). During the first phase of the project, six 5MW wind turbines generators (WTGs) are built in sub-area A. The distance between the WTGs is about 500m. Depths vary on this location from -25m TAW to -18m TAW. TAW is the Belgian reference system which islocated 0.18m below mean low low water spring (MLLWS), and 2.29m below mean sea level (MSL) in sub-area A. The tidal range at spring tide is about 4m.

GBFs have been chosen since the design is less sensitive to a particular wind turbine type. Monopiles would have been costly and very difficult to install because of the presence of dense sand layers and stiff clay below the seabed. The GBFs consist of concrete caisson structures ballasted with infill material. Each GBF is composed of a base plate (Ø 23.5m), a conical section (Ø 17m to 6.5m), a cylindrical section and a top plate. The top plate is situated at +17m TAW (Figure 2). The height of the structure varies according to the depth at each location.

Placement

The foundation level of each GBF is 3.50m below Reference Seabed Level (RSBL). The RSBL is defined as the lowest seabed level during the life time (30 years) of the foundation, including the effect of migrating sand waves and the erosion of the entire area.

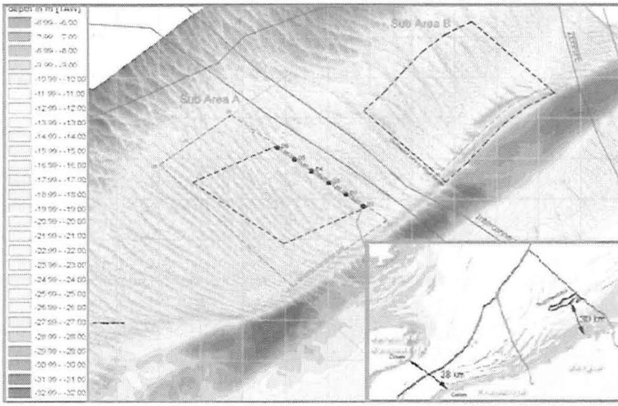

Figure 1 – Location of the 6 GBFs and bathymetry of the Thornton Bank.

For each GBF a foundation pit measured 50m x 80m at the bottom, is dredged some 4.8m below RSBL, with the main axis heading NE – SW. This lay-out is inspired by the prevailing current directions. Dredging occurred in two stages: (i) bulk dredging to remove the sand dunes and the top layer, followed by (ii) precision dredging to obtain a surface within the specified tolerances. On average, some 90000m^3 is dredged per foundation pit.

The foundation bed consist of two circular layers: (i) a filter layer from the dredged level up to 0.55m below foundation level, and (ii) a gravel layer up to target foundation level (Figure 2). The foundation beds are installed using a Dynamically Positioned Fallpipe Vessel. Per location, an average of 2500 tonnes of filter material and 1200 tonnes of gravel is placed. The maximum inclination of the gravel bed surface is <0.75° to assure verticality of the turbine towers and a proper transfer of the weight of the GBF to the subsoil. Precision levelling is achieved with a purpose designed tool, attached to the lower end of the fallpipe.

The GBFs are constructed onshore in Ostend. From there the foundations of about 3000 tonnes each, are transported towards the Thornton Bank by means of the heavy lift vessel *Rambiz*. At the location, the foundations are lowered on the previously prepared foundation bed. This is followed by the backfill and the placement of the scour protection.

THE SCOUR PROTECTION – DESIGN PROCES

The design of the scour protection is made for a 1 in 100 years return period. Design conditions are significant wave height H_{m0} = 6.3m, peak period T_p = 11s (duration 3 hours) and water level +1m TAW in combination with a maximum depth averaged current velocity of 1.2 m/s. Waves are non-breaking and waves and currents are assumed to be coincident. Maintenance has to be minimized and therefore a static design is chosen. Since for practical reasons, the stone size cannot vary from wind turbine to wind turbine, one stone size has been used. Stones should have a minimum weight of 2700kg/m^3 and a high crack resistance (e.g. >190MPa). The design of the scour protection is based on theoretical concepts and has been tested afterwards in a physical model. Due to restricted availability of material and execution methods, some modifications have been made afterwards.

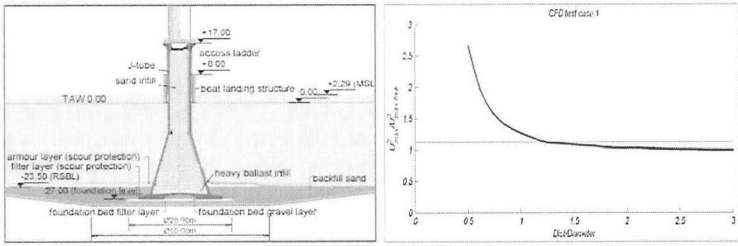

Figure 2 - Wind turbine foundation D6 (left); relative shear stress vs. the distance from the GBF centre (right).

Theoretical design

Given the design conditions and the water depth at each foundation, the required stone size for the armour layer is determined using the Shields criterion (Shields, 1936). As long as the Shields parameters due to waves and currents are smaller than the critical value, the stones are stable. For large grain size (dimensionless grain size D*>200, corresponding to diameter d>10mm for quartz grains in seawater), the critical Shields parameter equals 0.055 (Soulsby, 1997).

The calculation is performed for two locations: close to the GBF, and at the edges of the scour protection. Close to the GBF the current velocities are amplified due to the presence of the structure (factor 2 for a typical current profile around a pile); the bed is assumed to be flat here. For a 100 years return period, armour stones should have diameter 0.25m (or bigger) to be stable at the shallowest location (-18m TAW). At the edges the "normal" current velocities occur, in combination with a slope 1:5 of the armour stones. This leads to a reduction factor 0.75 of the critical bed shear stress, resulting in stones with a diameter $\geq$ 0.35m. The layer thickness of the armour layer is at least 2 times the median grain size D_{50}, which is 0.70m for this case (Hofmans and Verheij, 1997).

To guarantee a stable scour protection and to prevent stones sinking into the seabed, a filter layer is foreseen. A geometrically open filter is applied in order to avoid too strict criteria for the filter material, difficult placement and/or a second filter layer. The following filter material is proposed: standard grading 10/80mm, $D_{50,f}$ = 50mm with a wide gradation ($D_{85,f}/D_{15,f} > 5$). This has as consequence that the filter criteria for the original seabed material cannot be met. The coastal engineering manual (USACE, 2006) advises for these filters a thickness of at least 0.30m. However, to guarantee an effective clogging effect to stop migration of material through the filter pores and taking into the precision of bathymetric measurements, a minimum layer thickness of 0.60m was specified.

The extent of the scour protection has initially been chosen according to the guidelines in literature, mostly for monopiles. The diameter for the scour protection around a monopile is often taken at $4xD_{pile}$ (Sumer and Fredsoe, 2002; Escarameia, 1998). However, since the GBF is much wider and CFD modelling shows that an amplification factor = 1.12 of the shear stress is found at a distance of $1.2D_{GBF}$ (see figure 2) instead of at a distance $2xD_{pile}$ as for monopiles, the theoretical diameter of the scour protection could possibly be reduced to $3.5D_{GBF}$.

Physical Model

Physical model tests have been carried out at DHI (2007) to test the stability of the designed scour protection, the backfill and the filter bed during construction. The flume is 35m long, 5.5m wide and has a re-circulating current-flow generating system with generation of co-directional long-crested waves. Froude scaling law is applied and the tests are conducted at a linear scale of 1:52. The differences in densitiy of rock and water in model and nature were taken into account, and the gradings specified in the design were reproduced by combination of different gradations of sand and stones. The water depth in the model was 0.33m, corresponding to 17.18m in prototype. Since the backfill material is relatively too coarse for Froude scale modelling, the current is amplified by a factor 1.75-2.1 to obtain live-bed conditions. With such conditions, the scour in the backfill material will develop geometrically correct but with another time scale than calculated according to Froude scaling. So the time scale was corrected when interpreting the results. The velocity in the model varied from 1.2 to 3.6m/s.

The tests give an indication of the amount of scour to be expected in the backfill and the filter during construction. It is found that two big lobes form around the GBF under the average conditions, and that the filter material is vulnerable under moderate storm conditions, leading to local scour around the GBF (Bolle et al., 2009). This erosion pits also have consequences for the amounts of materials for the layer placed on top.

To check the armour stability tests are performed with the top of the armour layer 17m and 16m below the design water level. In both tests the armour layer was stable, although with the reduced water depth more erosion occurred at the outer rim of the protection (see Figure 3).

Scour protection lay-outs with different diameters are compared. Erosion occurred in all cases mainly at the rim, on the upstream side. The erosion is larger in tests with a reduced protection diameter, but the tests with diameters $2.5D_{GBF}$ (=37.5m) and $2D_{GBF}$ (=30m) show almost identical erosion. In all tests the rock displaced from the rim served as armour protection of the gentle outer slope.

Furthermore, the slope of the seabed at the edge of the scour protection is measured. In the performed tests a slope of about 1:4 developed.

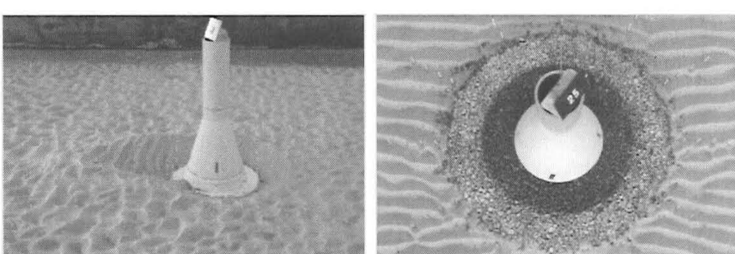

Figure 3 – left: backfill after test run with U_c=2.5m/s, without waves; right: scour protection with armour layer diameter 37.5m after 6 hours test with H_s=6.32m, T_p=11.6s, U_c=1.2m/s and water depth=17.18m.

First design proposal

Based on the results of the numerical and physical model tests a first design proposal is made. The scour protection system should be installed in four phases: (i) backfill of the foundation pits until -0.30m RSBL, (ii) installation of the filter layer (iii) installation of the armour layer up to maximum +1.00m RSBL and (iii) backfill of the area around the scour protection up to a level of +1.00m

RSBL (see Figure 4). The latter operation is proposed to create a smooth transition between the stones and the seabed, in order to minimise edge scour.

The characteristics of this design are summarised in Table 2. The extent of the filter layer is based on the diameter of the armour layer extended all around with about 2m to fully support the armour layer.

Besides the materials, layer thicknesses and extent; also execution tolerances are defined. The tolerances on the layer thickness are defined to guarantee the minimum required layer thickness. Therefore the tolerance on the filter layer thickness was defined as -0.0m and +0.25m, while for the armour layer thickness the tolerances were -0.0m and +0.35m. Concerning the diameter, only a minimum extent is defined.

For the geotechnical design of the GBFs the bottom levels that can be relied on should be specified. Therefore, a design line (see Figure 6) is defined based on following assumptions: the minimum level of the scour protection will be RSBL + 1.0m; the rim of the armour layer will smooth down to a slope of 1:5; at the edge of the scour protection 1m is taken downwards starting from RSBL; from this point on a critical slope (1:4) is taken based on the physical model tests. The further away from the edge of the scour protection, the less the local bathymetry will be affected. In order not to be too conservative the design line starts rising again after reaching a level of 7.0m below RSBL.

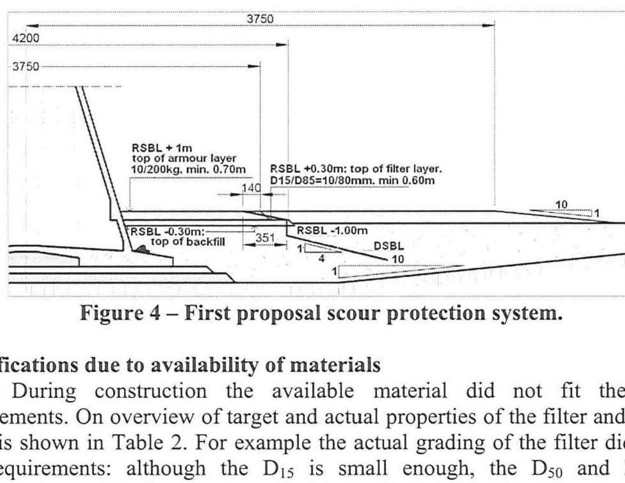

Figure 4 – First proposal scour protection system.

Modifications due to availability of materials

During construction the available material did not fit the initial requirements. On overview of target and actual properties of the filter and armour layer is shown in Table 2. For example the actual grading of the filter did not fit the requirements: although the D_{15} is small enough, the D_{50} and D_{85} are significantly smaller than those required in the final design. The advantage of the small D_{50} is a positive effect on the stability of the geometrically open filter.

To guarantee good functionality, this filter is however only acceptable in combination with a 10/200kg grading for the armour layer. A suitable grading for the armour layer is obtained by mixing 80% 40/200kg with 20% 5/40kg grading. Using this final armour grading, the filter rules between armour and filter material for a geometrically closed filter are fulfilled.

Concerning the extent of the scour protection, $2.5xD_{GBF}$ is not enough for geotechnical purposes. Due to edge scour, material (and thus weight) will disappear around the scour protection. To guarantee the stability of the foundations, the extent is increased to 44 to 58m, depending on location.

Table 1: Target and actual material specifications of the scour protection

target and actual specifications scour protection *(when different: actual in italics)*			
		filter layer	**armour layer**
mate-rial	**type**	crushed gravel *(hard, compact limestone rock)*	stones *(hard, compact limestone rock)*
	dimen-sions	10/80mm, D_{50} = 50mm, wide gradation $D_{85}/D_{15} > 5$ *(0/120mm, standard quarry material)*	10/200 kg, D_{50} = 350mm, wide gradation $D_{85}/D_{15} >5$ *(5-40kg and 40-200kg: 20% / 80% stone mixture)*
layer thickness or level		min. 0.60m	min 0.70m, top level = RSBL +1.30m / 1.45m
diameter or extent of layer		diameter min 42.0m *(48.5-62.5m for geotechnical purposes)*	diameter min 37.5m (=2.5D_{GBF}) *(44-58m for geotechnical purposes)*

Modifications due to execution methods

Based on discussions with the Contractor the first proposal is optimised to obtain a more economical execution. The installation of the scour protection in 4 phases was too time consuming and one stage is eliminated by installing the scour protection on top of the backfill installed up to RSBL. As a result the total scour protection is situated above the surrounding seabed. This implies that edge scour can become more important, and should be closely monitored. On the other hand this solution provides more weight on the edges of the foundation, which positively contributes to the overall stability of the GBFs. Allowing this modification requires execution tolerances to be strictly met in order to guarantee the stability of the armour stones under the design conditions. Not achieving the tolerances would lead to a too high top level of the armour layer, resulting in an instable armour layer at the shallowest locations.

For the area with the cable entrances it is discussed that additional scour protection should be installed over an area of at least 10m wide and 15m further from the GBF (see Figure 5). This adjustment is needed in order to guarantee the required cable burial depth of 2m.

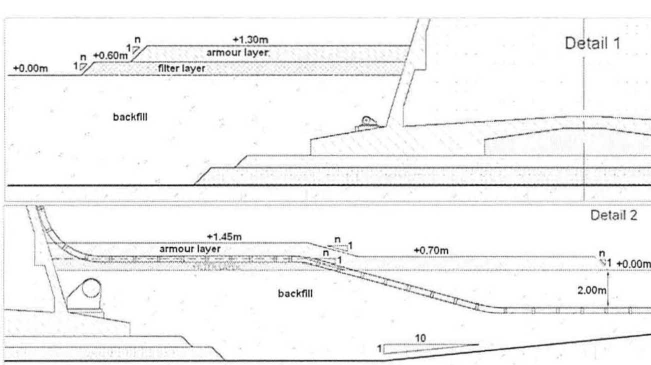

Figure 5 – modified scour protection system: detail 1 - normal configuration; detail 2 - at cable entry.

The tolerances for construction of the scour protection are defined to assure the minimum specified layer thickness, which is needed to guarantee the design seabed level for the geotechnical design. The originally defined tolerances of -0/+0.25m on the filter layer thickness and -0/+0.35m on the armour layer thickness are maintained, although hard to accept by the contractor.

Placement of the scour protection according to the method statement

The scour protection works are executed with an automotive fallpipe barge equipped with a fallpipe for rock placement and assisted by two anchor handling and general support vessels. One of these support vessels is equipped with a multi-beam survey launch. The automotive fallpipe barge has a main deck cargo hold capacity of approximately 3000T of rock materials, and has also been used for the backfill around the GBFs and the hydraulic infill of the GBFs. Furthermore a supply vessel, capable of transporting 2000T of rock material, was used for the supply, offloading and transfer of filter materials and armour stones. The hopper well of this vessel is equipped with an appropriate protection system against impact damage, especially when handling the armour rock stones.

Prior to the start of the offshore execution, stock piles of both filter and armour material are made onshore on a quay wall. These materials are then loaded inside the hopper well, from where they are transferred onto the main deck cargo hold of the automotive fallpipe barge by means of an offloading crane installed on board the supply vessel, while moored alongside the barge. The supply vessel is kept securely moored via the two constant tension mooring winches installed on the main deck of the barge, allowing easy offloading of filter and armour materials.

Six computer-controlled, hydraulically driven anchor winches allow movement along a predefined track. The six anchors are placed in advance and consisted of two 12T Delta Flipper anchors (bow and aft anchor), and four 9T Delta Flipper side anchors. One location is divided in six segments. For each segment a different anchor pattern is applicable, where positioning and tracking of the barge is executed by means of the 6 winches.

These are automatically controlled by a computer system that uses as input, among others, the LRK satellite positioning system and the gyrocompass installed on board. This continuously provides the actual position of the barge.

For storage of the rock materials on deck of the barge, a rectangular cargo hold is created by means of 2 meter high cargo hold coamings. This cargo hold is accessible for the materials handling crane for further manipulation of the materials inside the hold. Filter materials and armour rock are transferred from the cargo hold towards the fallpipe's feeding hopper using a conveyor belt and vibratory feeder system. The materials are discharged into the fallpipe chute and fall inside the fallpipe towards the seabed. A weighing device is installed at a belt section and included in the conveyor belt system, allowing the continuous monitoring of the rock quantities transferred and installed. This data serves as an input for the computer controlled automotive moving of the fallpipe barge along a predefined stone dump track.

The fallpipe height (typically 1 to 2 m above the target level of the layer to be realized) is automatically corrected for tidal fluctuations and swell using a hydraulic winch system steered by the board computer and supplied with the actual z elevation from the LRK satellite positioning system. Intermediate bathymetric surveys are performed after completion of each intermediate layer and the updated seabed survey introduced into the hauling computer.

In a first step a filter layer is placed in all sectors, after which the armour layer followed (in reverse order). Armour installation works excluded initially the installation of rock material in the segments at the bell-mouth locations and along the cable routes. At those locations, the armour layer is only placed after the installation of the cables. At the J-tube positions a trench is left open in order to ensure a smooth cable pull-in. After the cable installation (with cable protectors) the scour protection is then finalized.

MONITORING PROGRAM

During construction

The seabed around the foundations is extensively monitored during the works. For the six GBF's, multi-beam surveys are available from the seabed before the works, as well as the in- and out surveys of the different stages of construction, such as dredging of the foundation pit (April 2008), placement of the filterbed, gravelbed, GBF, backfill, filter and armour (end of January 2009). For the same period the hydrodynamic conditions are available from the stations from the Flemisch banks monitoring network, and an additional directional wave buoy installed on the Thornton Bank.

Operation and Maintenance program (O&M)

The O&M program consists of the execution of a multi-beam bathymetric survey of the scour protection and surrounding seabed in an area of 200m diameter around the six GBFs. This survey will be executed twice a year, at the start and the end of the good weather period, with roughly 6 months in-between each other. To verify the possible seabed evolutions in between the new foundations and to monitor the morphological evolution of the Thornton Bank as a natural feature, the inspection program shall once a year include a bathymetrical survey of a wider zone. This zone comprises next to the cable routing, also an area of 2700m (NW-SE direction along the centre points of the GBFs) by 800m. The first bathymetrical follow-up survey was executed in September 2009.

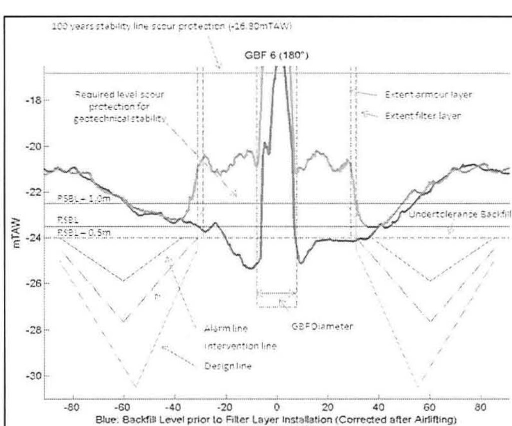

Figure 6: Concept of alarm line, intervention line and design line.

MONITORING RESULTS

During construction

The wave data from the Thornton Bank have been used for the analysis of the stability of the backfill material in relation to summer storm exposure and the stability of the (temporary exposed) filter material in late autumn, begin winter. The backfill and filter behaved during exposure very much as expected. Lobes were formed in the backfill, and local scour around the GBF in the filter was observed, as predicted with the physical model tests (Bolle et al. 2009).

Layer thicknesses are evaluated based on the in- and outsurveys. Figure 6 compares for one cross section the situation prior to the installation of the scour protection with the final out-survey after all works were finished. This type of figure is used to evaluate the different steps of the works. With regard to the stability of the scour protection itself, the level below which the scour protection should remain in order to guarantee the stability during the 100 years return period event is also indicated. For GBF 6 it can be seen from the figure that the top of the armour stays well below the stability line for the scour protection. However, the top of the scour protection lies about 2m above the minimum required level (RSBL +1m), which could be unfavourable for edge scour.

During operation

Obviously, the design line should not only be guaranteed by the end of the works, but also during the entire project's lifetime. Therefore, a dedicated monitoring program has been set up. Distinction is made between two areas: the area above the scour protection and the remaining area inside a diameter of 150m.

In the first area, i.e. close to the structure, displacement of the armour rock is allowable but the level should be at least 1.0m above RSBL. If in a zone the first layer of the armour stones is eroded over an area of 4 x D_{n50}^2 (with D_{n50} = the nominal diameter) without the filter layer being exposed, an alarm situation is reached. If in a zone the first layer of the armour stones is eroded over an area of 8 x D_{n50}^2 without the filter layer being exposed, an intervention situation is reached. The system is damaged when the second layer of armour stones is absent and the filter layer is exposed.

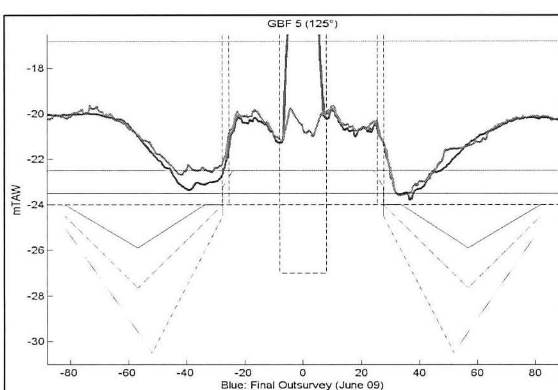

Figure 7: Cross section comparing outsurvey June 2009 (blue) with first monitoring results September 2009 (red).

To evaluate the second area, two lines related to intervention decisions are defined in addition to the design line: the alarm and intervention line. The slope of the intervention line is twice as gentle as the one of the design line: 1:8 instead of 1:4. The slope of the alarm line is 1:12. Both lines are also indicated in Figure 6.

Based on the alarm – intervention – design line concept results of monitoring campaigns can quickly be evaluated and it can easily be examined if further action is required. After the final out-surveys in June 2009, one monitoring campaign took place, namely in September 2009. A typical cross section comparing the results of both surveys is given in Figure 7. From the survey results it can be concluded that in the summer months no significant edge scour did occur, if at all. Instead, it seems that there is a sedimentation tendency in some parts. Hence, the first monitoring campaign showed no need for any urgent action.

CONCLUSIONS

During the first phase of C-Power's wind farm project, the scour protection design has been optimised. Starting from the theoretical design, supported by physical model tests, numerous discussions with the contractor resulted in a more economical design. It became important to minimise the operational time on sea, which led to the elimination of the second phase of the backfill. However, even with state of the art equipment, it was very difficult to perform the scour protection installation on the North Sea within the specified tolerances. Maintaining a minimum layer thickness (to guarantee stability), without placing too much material (to avoid rising costs) is still a point of interest. For future designs, these aspects should be addressed right from the start. For the GBFs already in place on the Thornton Bank, the first monitoring results showed a stable behaviour of the scour protection and the seabed around. Nevertheless, monitoring continues to be able to intervene in time, if necessary.

ACKNOWLEDGEMENTS

We gratefully acknowledge C-Power, for providing the wave measurements and the bathymetric surveys at the different stages of the works.

REFERENCES

Bolle A., Haerens P., Trouw K., Smits J. and Dewaele G. (2009) "Scour around gravity-based wind turbine foundations - prototype measurements." *Proc. Coasts, Marine structures and Breakwaters conference*, 2009, Edinburgh.

DHI (2007). "Wind Farm Thornton Bank, Belgium; 3D Scour Protection Tests."

Escarameia M. (1998). "Laboratory Investigation of scour around large structures in tidal waters." HR Wallingford.

Hoffmans, G.J.C.M. and Verheij, H.J. (1997). "Scour Manual." AA Balkema Publications, pp. 1-205.

Shields. A (1936). Anwendung der ähnlichkeits-mechanik und der turbulenzforschung auf die geschiebebewegung. Preussische versuchsanstalt für wasserbau und schiffbau, vol.26, Berlin.

Soulsby R.L. (1997). "Dynamics of marine sands. A manual for practical applications." *Report SR466*. HR Wallingford.

Sumer B.M. and Fredsoe J. (2002). "The mechanics of scour in the marine environment." *Advanced series on Ocean Engineering*, Vol. 17, pp. 1-536.

USACE (2006). "Coastal Engineering Manual (CEM)."